1   **Assessing the biomineralization processes in the shell layers of**

2   **modern brachiopods from oxygen isotopic composition and elemental**

3   **ratios: Implications for their use as paleonvironmental proxies**

4

5   Claire Rollion-Bard[1*], Sara Milner Garcia[1], Pierre Burckel[1], Lucia Angiolini[2], Hana

6   Jurikova[3], Adam Tomašových[4], Daniela Henkel[3]

7

8   [1]Institut de Physique du Globe de Paris (IPGP), Sorbonne Paris-Cité, Univ Paris

9   Diderot, CNRS, F-75005 Paris, France

10 [2]Dipartimento di Scienze della Terra "A. Desio", Università degli Studi di Milano,

11 Milan, Italy

12 [3]GEOMAR Helmholtz Centre for Ocean Research Kiel, 24148 Kiel, Wischhofstr. 1-3,

13 Germany

14 [4]Earth Science Institute, Slovak Academy of Sciences, Dúbravská cesta 9, 84005

15 Bratislava, Slovakia

16 *Corresponding authors: rollion@ipgp.fr

17

18 Keywords: Brachiopod, oxygen isotopes, element-to-calcium ratios, shell

19 microstructure, vital effects, proxy.

20

21   **Abstract**

22   Fossil brachiopod shells are often used as valuable archives to reconstruct

23   paleoenvironmental conditions in deep time. However, biomineralization processes

24   can impact their fidelity as geochemical proxies. Brachiopod shells comprise an outer

25   primary layer, a secondary fibrous layer and sometimes, a tertiary columnar layer.

26   Therefore, it is essential to assess the potential effects of the biomineralization

27   processes in each of the different shell microstructures of modern brachiopods. This

28   study analyses the oxygen isotopic composition together with Li/Ca, Na/Ca Mg/Ca

29   and Sr/Ca data at high spatial (20-50µm) resolution in seven modern brachiopod

30   species, focusing on differences between the primary, secondary and tertiary layers. In

31   all studied species, $\delta^{18}O$ values of the outer primary layer are consistently out of

32   equilibrium with seawater. Also, this shell layer is enriched in Li, Na, Mg and Sr.

33   Contrary to the primary layer, the innermost secondary layer is near or at oxygen

34   isotopic and elemental equilibrium with ambient seawater. The columnar tertiary shell

35   layer, if present, has the least variable and the heaviest oxygen isotopic composition,

36   within the range of equilibrium values with seawater. This tertiary layer, however, is

37   depleted in minor and trace elements relative to the other shell layers. Thus, the

38   tertiary layer is more suitable for oxygen isotopic studies, whereas the innermost

39   secondary layer of the most mature parts of the shell is the best target in two-layered

40   shells. While we do not observe any clear interspecific relationships between Mg/Ca

41   and Sr/Ca ratios, on one hand, and environmental parameters such as temperature,

42   salinity and pH, on the other hand, there is a positive interspecific relation between

43   Na/Ca and salinity and a negative interspecific relation between Li/Ca and

44   temperature, suggesting their potential use as proxies of physicochemical parameters

45   of seawater.

46

1. Introduction

Temporal changes of seawater temperature, salinity and pH during the Phanerozoic can leave signatures in the geological record, offering an exceptional opportunity to reconstruct past conditions in seawater chemistry, to understand the on-going climate change and to predict its potential effects in the near future. Biominerals produced by marine calcifying organisms are a key tool in reconstructing the environmental parameters during their lifetime, as they act as archives of environmental conditions that prevail during their growth. To date, most of the information on the chemical evolution of marine environments through the Phanerozoic is derived from stable isotopes and trace element data of marine calcifying organisms such as foraminifera, corals, bivalves and brachiopods (e.g Veizer et al., 1999; Lea et al., 2000; Angiolini et al., 2009; Brand et al., 2011; Schöne and Surge, 2012; Crippa et al, 2016b; Garbelli et al., 2016). Brachiopods were ubiquitous throughout the Phanerozoic and continuous in the fossil record since the Early Cambrian up to now (Williams, 1997; Zhang et al., 2008). Most of them secrete shells made of low-magnesium calcite, generally the diagenetically most resistant (e.g. Lowenstam, 1961; Brand and Veizer, 1980; Popp et al, 1986). Therefore, the isotopic compositions and element/Ca ratios derived from fossil brachiopod shells are a powerful tool in paleoenvironmental studies (e.g. Popp et al., 1986; Brand, 1989; Veizer at al., 1999; Steuber and Veizer, 2002; Ullmann et al., 2016). Lowenstam (1961) showed that modern brachiopods precipitate their shells in oxygen isotopic equilibrium with ambient seawater and since then, fossil brachiopod shells have been extensively used to reconstruct temperature of ancient oceans (e.g. Bates and Brand, 1991; Grossman et al., 1993; Wenzel and Joachimski, 1996; Korte et al., 2008). In the

72 meantime, several studies on the incorporation of oxygen isotopes in modern

73 brachiopod shells have been conducted in order to verify the assertion of Lowenstam

74 (1961) (e.g. Carpenter and Lohmann, 1995; Buening and Spero, 1996; Brand et al.,

75 2003; Parkinson et al., 2005). They concluded that the calcite fibres of the secondary

76 layer incorporate oxygen isotopes in equilibrium with seawater, while the primary

77 layer is always depleted in ^{18}O relative to equilibrium values. Recent studies carried

78 out with high spatial resolution techniques (Auclair et al., 2003; Yamamoto et al.,

79 2010, 2013; Cusack et al., 2012; Takayanagi et al., 2012, 2013; Romanin et al., 2018)

80 observed that the oxygen isotopic equilibrium is only reached in the innermost part of

81 the secondary layer, while the outermost part is depleted in ^{18}O relative to

82 equilibrium. The depletion of ^{18}O in the primary and outermost part of the secondary

83 layer is explained by kinetic fractionation effects (e.g. Auclair et al., 2003; Yamamoto

84 et al., 2010, 2013; Cusack et al., 2012). However, except in Cusack et al. (2012), all

85 of the previous analyses investigated the intrashell variations in stable isotopes with

86 micromill transects, achieving a relatively coarse resolution of about 0.1 – 0.5 mm. At

87 such resolution, seasonal or growth rate difference can be averaged out. In addition,

88 little attention has been paid to three-layered brachiopod species. In fossil

89 brachiopods, the tertiary layer probably achieves a more stable oxygen isotopic

90 composition and lower trace element contents than the primary and secondary layers

91 (Grossman et al., 1996; Angiolini et al., 2012), in agreement with the findings of

92 Romanin et al. (2018) for modern brachiopods.

93 Only few studies focused on the incorporation of elements in the different

94 brachiopod microstructures of the shells. Mg/Ca of brachiopod calcite has been

95 suggested to have a consistent temperature dependency with ambient seawater by

96 different studies (Perez-Huerta et al., 2008; Powell et al., 2009; Brand et al., 2013;

97   Butler et al., 2015). However, as most of the brachiopods precipitate low-magnesium

98   calcite shells (e.g. Clarke and Wheeler, 1917), the assertion that Mg/Ca can be used as

99   temperature proxy has been challenged by other studies demonstrating that

100 magnesium incorporation into the calcite shell is mainly controlled by physiological

101 effects rather than environmental parameters (Lowenstam, 1961; Buening and

102 Carlson, 1992; England et al., 2006; Cusack et al., 2008). As for Mg/Ca ratio, Sr/Ca

103 and Li/Ca ratios have also been proposed as seawater temperature proxy (Delaney et

104 al., 1989; Lowenstam and Weiner, 1989).

105   To use elemental ratios and $\delta^{18}O$ values of brachiopod shells as environmental

106 proxies, it is fundamental to know the processes involved in their incorporation, and

107 to determine their reliability. Here, we investigated the variations of $\delta^{18}O$ values and

108 elemental ratios (Li/Ca, Na/Ca, Mg/Ca and Sr/Ca) between the three layers differing

109 in microstructure, using high spatial resolution techniques (ion microprobe and laser

110 ablation-inductively coupled plasma-mass spectrometry, LA-ICP-MS). This

111 investigation was performed on seven brachiopod species belonging to the orders

112 Rhynchonellida and Terebratulida.

113

114 **2. Materials and methods**

115

116   Four specimens of *Magasella sanguinea* (Leach, 1814) (specimens DS401L,

117 DS402L, DS403L and DS404L), three of *Terebratalia transversa* (Sowerby, 1846)

118 (D500L, D501L and D504L), *Notosaria nigricans* (Sowerby, 1846) (DS428L,

119 DS429L and DS430L) and *Gryphus vitreus* (Born, 1778) (GV13, GV47 and GV78),

120 two specimens of *Magellania venosa* (Dixon, 1789) (MV05 and MV17) and one

121 specimen of *Liothyrella neozelanica* (Thomson, 1918), (DS422L) and *Calloria*

122 *inconspicua* (Sowerby, 1846) (DS419L) were selected. In total, we analysed

123 seventeen specimens from seven modern brachiopod species (Fig. S1). *Terebratalia*

124 *transversa* samples were collected at a depth of 64m in the subtidal zone of San Juan

125 Islands, Washington, USA (48.5°N, 123°W) in February 2002. *Magellania venosa*

126 was collected in Ensenada de las Islas, Chile (43.8°S, 72.9°W) in March 2013, at a

127 depth of 22m. *Gryphus vitreus* shells were sampled in 1974 near Tuscan Archipelago,

128 Italy (42.3°N, 9.9°E) at a water depth between 140 and 160m. Finally, *M. sanguinea*,

129 *C. inconspicua*, *L. neozelanica* and *N. nigricans* were collected in August 2010 from

130 the subtidal zone of Doubful Sound, New Zealand (45.4°S, 167.1°E) at a depth of

131 20m. They were collected in environments differing in water depth and latitude, and

132 thus covering a wide range of environmental settings in terms of temperature, salinity

133 and pH (Fig. 1, Table 1).

134

135 *2.1. Sample preparation*

136   The shells of each specimen were disarticulated into valves. The valves were

137 cut into halves along a midline from the posterior (umbo) to the anterior parts to

138 obtain longitudinal sections that are parallel with the ontogenetic growth. One portion

139 of ventral and/or dorsal valves was mounted in epoxy and polished with diamond

140 paste down to 1µm (Fig. 2), and then used for ion microprobe and LA-ICP-MS. The

141 other portion was kept for bulk $\delta^{18}O$ analyses, carried out by milling. In that case, any

142 remaining soft tissue and encrusting organisms, such as bryozoans or coralline algae,

143 were removed manually and cleaned in an ultrasonic bath with MilliQ water for 30

144 minutes. Later, they were brushed and rinsed with deionized water and then dried at

145 ambient temperature.

146

2.2. Scanning electron microscopy (SEM)

For the microstructural investigation of the brachiopod shell, the polished samples were etched with 5% hydrochloric acid for 3 seconds (Crippa et al., 2016a) and then carbon coated. Images were performed using a Zeiss-Auriga scanning electron microscope (SEM), equipped with a field emission electron gun (FEG) at 15 KeV with a SE-Inlens detector.

153

2.3. Oxygen isotopic analysis

155

2.3.1. Ion microprobe technique

Oxygen isotopic composition was determined using the ion microprobe technique with a CAMECA IMS 1280-HR at CRPG-CNRS (Nancy, France) during 4 analytical sessions. Analyses were carried out following the procedure as described in Rollion-Bard et al. (2007). Oxygen isotopic analyses were performed with a 5 nA Cs^+ primary beam with a charge compensation by a normal-incidence electron gun. The oxygen isotopes, ^{16}O and ^{18}O, were simultaneously measured in multicollection mode by using two off-axis Faraday cups, L'2 and H1. Gains of Faraday cups were intercalibrated at the beginning of each analytical session. Analyses were performed with a pre-sputtering time of 30 seconds, followed by 30 cycles of 4 seconds. During the pre-sputtering time, backgrounds of the Faraday cups were measured. Typical ion intensities of around 6 x 10^6 cps (counts per second) and 3 x 10^9 cps were obtained for $^{18}O^-$ and $^{16}O^-$, respectively, and after few minutes of counting, the internal $2\sigma_n$ error was less than ±0.1‰. The instrumental mass fractionation (IMF) was corrected by

170   normalizing to three in-house calcite standards, BRET ($\delta^{18}O$=-10.87‰ V-PDB,

171   Rollion-Bard and Marin-Carbonne, 2011), MEX ($\delta^{18}O$ = -7.05‰ V-PDB, Rollion-

172   Bard et al., 2007) and CCciAg ($\delta^{18}O$ = -11.61‰ V-PDB). The external

173   reproducibility, estimated from replicates of the calcite in-house standards was

174   between ±0.10 and 0.55‰, depending on the analytical session. The total error for

175   each $\delta^{18}O$ measurement takes into account the internal error and the external

176   reproducibility. When necessary, the IMF was also corrected for the Mg content

177   effect, by applying the correction factor of -0.3 x MgO %wt (Rollion-Bard and Marin-

178   Carbonne, 2011). All $\delta^{18}O$ values are presented in ‰ relative to V-PDB international

179   standard.

180   To assess the variability in oxygen isotopic composition, transects from the

181   outermost to the innermost part of the shell were performed with spot of 20 µm and

182   applying a constant step of 50 µm. They were carried out in the central and/or anterior

183   parts of each shell (see Fig. 3 for an example of transect in *N. nigricans*), with a

184   distance of 6 mm (*N. nigricans*) to 17 mm (*M. venosa*) between them, depending on

185   the shell size. The number of analyses was determined by the shell thickness and

186   converted into relative distance to have the best comparison between transects, i.e. 0%

187   represents the outermost part of the shell and 100% the innermost. In some cases, the

188   different shell layers could not be analysed due to their low thickness compared to the

189   spot size of the ion microprobe or laser ablation measurements. Moreover, as it was

190   shown by previously studies (Parkinson et al, 2005; Brand et al, 2015; Romanin et al,

191   2018; Ye et al, 2019) that there are no significant differences between ventral and

192   dorsal valves, the profiles were not performed in all ventral and dorsal valves. The

193   analysed transects were later observed under SEM to assign each spot to a specific

194   shell layer.

195

2.3.2. Conventional bulk technique

Oxygen isotopic compositions of brachiopod shells were analysed by conventional bulk technique, in order to check the accuracy of the $\delta^{18}O$ values measured with the ion microprobe. For this, the anterior part of the other half of each shell (Fig. 2) was sampled using a Merchantec MicroMill (New Wave Research). The different shell layers were micromilled until obtaining around 30 µg of powder. The primary layer was first sampled by carving lines at the surface with a depth of around 30 µm. In two-layered shells, the secondary layer was drilled. In the case of *L. neozelanica*, as the secondary and tertiary layers are often intercalated (Fig. 4), the powder was a mixture of tertiary and secondary layers. For *G. vitreus*, lines were performed in the central part to obtain mainly the tertiary layer. Calcite powders were then reacted with 100% phosphoric acid at 25ºC and measured by a Gas Bench coupled to a Thermo Finnigan DELTA Plus XP isotope ratio mass spectrometer at IPGP, France. $\delta^{18}O$ and $\delta^{13}C$ data are presented in Table 3. The average of the ion probe $\delta^{18}O$ values of the anterior transects of each sample was compared to the bulk value and the values were adjusted. Depending on the analytical session, an offset from 0.84 to 4.44‰ between the ion probe and bulk analyses was observed, similar to the offset reported by Kolodny et al. (2003), Cusack et al. (2012) and Juillet-Leclerc et al. (2018). The causes of this offset are not determined yet. Nevertheless, the difference of $\delta^{18}O$ values between the primary and secondary layers was in agreement with the two techniques, giving confidence to the intra-shell variability measured with the ion microprobe technique.

218

2.4. Elemental measurements by LA-ICP-MS

220   Chemical composition (Li, Na, Mg, Al, Ca and Sr) was analysed with an

221   Analyte G2 Excimer laser ablation system (193 nm), coupled to a quadrupole Agilent

222   7900 ICP-MS (LA-ICP-MS). It was operated at a repetition rate of 5 Hz and an

223   energy fluence of 3.37 Jxcm^{-2}. Samples were analysed using a laser spot of 50µm

224   diameter and each measurement consisted of 60 seconds with a measurement of the

225   background (gas blank) of 30 seconds. The isotopes ^{7}Li, ^{23}Na, ^{24}Mg, ^{25}Mg, ^{27}Al, ^{43}Ca,

226   ^{44}Ca, and ^{88}Sr were monitored. ^{27}Al was collected to check any contamination by clay

227   minerals that could shift Mg/Ca values upwards (Barker et al., 2003). One run

228   comprised 10 to 20 analyses, depending on the shell thickness of the sample. Due to

229   the thickness of the primary layer relative to the laser spot size, it was not always

230   possible to analyse it, as for example for *Gryphus vitreus*.

231   Measurements of NIST glass standards 610 and 612 were acquired before and after

232   each run. The use of NIST glasses as standards for carbonate analyses was shown

233   suitable and not subject to matrix effects (e.g. Sylvester, 2008). Raw counts were

234   processed using IOLITE software with NIST glasses used for calibrating the elements

235   and ^{43}Ca as an internal standard. The overall precision (RSD, Relative Standard

236   Deviation) of elemental ratios (TE/Ca), based on repeated measurements of NIST 612

237   glass, was calculated by adding the errors of the specific element (σ_x) and the error of

238   Ca (σ_{Ca}), as RSD=$(\sigma_x^2 + \sigma_{Ca}^2)^{1/2}$, and was 14% for Li/Ca, 7% for Na/Ca, 4% for

239   Mg/Ca and 2% for Sr/Ca.

240

241   **3. Results**

242

243   *3.1. Shell microstructure*

244   Shells of rhynchonelliform brachiopods comprise up to three calcite layers

245   (Williams, 1966): the outer primary layer, made by acicular calcite, the secondary

246   fibrous layer and sometimes a tertiary columnar layer (e.g. Williams, 1997;

247   Griesshaber et al., 2005; Immenhauser et al., 2016). The three different shell

248   microstructures can be observed under SEM (Fig. 4). In all brachiopod species, a thin

249   outer primary layer of ~20µm thickness, made of finely acicular and granular calcite

250   was observed. Adjacent to the outer primary layer, a secondary layer made by calcite

251   fibres forms the majority of the shells, except for *G. vitreus* specimens. The thickness

252   of the secondary layer varies between species and specimens, from 0.3 to 1.4 mm. A

253   tertiary layer made of columnar calcite is developed in *L. neozelanica* and *G. vitreus*

254   (Fig. 4c). In *G. vitreus*, the shell consists almost exclusively of tertiary layer, while in

255   some areas of the *L. neozelanica* shell, the production of the tertiary layer is reverted

256   into secondary layer again (Fig. S2). Endopunctae - characteristic perforations of the

257   shell - were also evident in the secondary layer of terebratulid brachiopods (Fig. 4a),

258   whereas they were absent in the rhynchonellid *N. nigricans* (Fig. 4b), as expected

259   (e.g. Perez-Huerta et al., 2009).

260

261   *3.2 Geochemical compositions of brachiopod shell microstructure*

262   Carbon isotopic compositions are between -1.8 and 2.8‰, depending on the

263   species (Table 3). These values are in agreement with Brand et al (2015). Values of

264   δ^{13}C of *G. vitreus* (between 2.7 and 2.8‰) seem to plot in the equilibrium field as

265   defined by Brand et al (2015). The δ^{13}C values of the other species vary between

266   individuals (Table 3). This could be due to incorporation of carbon in disequilibrium

267   from transition zone calcite as defined by Brand et al (2015).

268   All SIMS $\delta^{18}O$ and minor and trace element values are listed in the

269   supplementary tables. Transects were performed in the central and anterior parts (Fig.

270   3) and throughout the different microstructures from the outermost to the innermost

271   shell.

272

273   *3.2.1. Primary layer (PL)*

274   In terebratulid brachiopods, the primary layer is generally depleted in ^{18}O

275   relative to the secondary and tertiary layers (Fig. 5), as previously reported (e.g.

276   Carpenter and Lohmann, 1995; Auclair et al., 2003; Parkinson et al., 2005; Cusack et

277   al., 2012). The variability within the primary layer is as high as 2.5‰, in agreement

278   with Auclair et al. (2003) and Carpenter and Lohmann (1995). In *T. transversa*, $\delta^{18}O$

279   values of the primary layer range from -5.7 ± 0.2‰ (dorsal valve of specimen D501L)

280   to -3.2 ± 0.2 (ventral valve of D500L), even if the majority of the $\delta^{18}O$ values of the

281   primary layer are around -3‰. In *M. sanguinea* and *C. inconspicua*, collected at the

282   same location, it ranges from -4.2 ± 0.2‰ to -1.0 ± 0.4‰ (DS402L) and from -3.9 ±

283   0.4‰ to -3.2 ± 0.4‰ (DS419L). In the primary layer of *M. venosa*, $\delta^{18}O$ values are

284   between -5.6 ± 0.2‰ (ventral valve of MV05) and -2.3 ± 0.2‰ (dorsal valve of

285   MV17). In the rhynchonellid brachiopod *N. nigricans*, the primary layer is not as

286   depleted in ^{18}O as in terebratulid brachiopods. The intrashell variability is less

287   pronounced, with $\delta^{18}O$ values between -1.0 ± 0.3‰ (DS429L) and 0.7 ± 0.2‰

288   (DS430L). $\delta^{18}O$ values of the primary layer of three-layered brachiopods are -3.8 ±

289 0.3‰ in *L. neozelanica* and from -2. ± 0.2‰ (ventral valve of GV47) to 0.5 ± 0.2‰

290 (dorsal valve of GV47) in *G. vitreus*.

291 Elemental ratios of the primary layer are generally higher than in secondary

292 and tertiary layers (Fig. 6). In rhynchonelliform brachiopods, the higher content of

293 trace elements in the primary layer is well known (England et al., 2006; Cusack and

294 Williams, 2007; Perez-Huerta et al., 2008). However, the enrichment is more

295 pronounced in the rhynchonellid *N. nigricans* than in terebratulid species (Fig. 6).

296 In the primary layer, Li/Ca values range from 27.8 ± 3.5 to 36.5 ± 5.5

297 µmol/mol in *T. transversa*, from 31.9 ± 5.3 µmol/mol to 33.8 ± 5.6 µmol/mol in *M.*

298 *sanguinea,* 38.6 ± 5.8 µmol/mol in *C. inconspicua,* from 36.1 ± 5.3 to 55.5 ± 6.1

299 µmol/mol in *M. venosa,* from 35.9 ± 5.3 to 36.5 ± 5.6 µmol/mol in *L. neozelanica*,

300 from 33.1 ± 6.1 µmol/mol to 43.5 ± 5.4 µmol/mol in *G. vitreus* and from 36.8 ± 4.7 to

301 41.9 ± 5.0 µmol/mol in *N. nigricans*.

302 Na/Ca values in *T. transversa* are between 10.2 ± 0.4 and 14.0 ± 0.3

303 mmol/mol, in *M. sanguinea* between 13.8 ± 0.3 and 14.3 ± 0.4 mmol/mol, in *C.*

304 *inconspicua* is 17.6 ± 0.6 mmol/mol, in *M. venosa* between 15.5 ± 0.5 and 15.6 ± 0.3

305 mmol/mol, in *L. neozelanica* between 12.6 ± 0.3 mmol/mol and 22.6 ± 1.5 mmol/mol,

306 in *G. vitreus* is between 14.4 ± 0.3 mmol/mol and 18.3 ± 0.4 mmol/mol and in *N.*

307 *nigricans* between 15.0 ± 0.3 mmol/mol and 16.3 ± 0.3 mmol/mol.

308 Mg/Ca values in the primary layer range from 5.1 ± 0.1 to 10.2 ± 0.5

309 mmol/mol in *T. transversa*, from 10.3 ± 0.3 to 11.3 ± 0.4 mmol/mol in *M. sanguinea,*

310 15.6 ± 0.6 mmol/mol in *C. inconspicua,* from 5.3 ± 0.1 to 9.8 ± 0.2 mmol/mol in *M.*

311 *venosa,* from 15.6 ± 0.4 to 24.6 ± 0.7 mmol/mol in *L. neozelanica*, from 15.4 ± 0.3 to

312   39.8 ± 0.6 mmol/mol in *G. vitreus* and from 19.1 ± 0.3 to 21.3 ± 0.5 mmol/mol in *N.*

313   *nigricans.*

314   Finally, Sr/Ca values in *T. transversa* are between 1.54 ± 0.05 and 1.85 ± 0.08

315   mmol/mol, in *M. sanguinea* between 1.70 ± 0.04 and 1.71 ± 0.06 mmol/mol, in *C.*

316   *inconspicua* is 2.35 ± 0.08 mmol/mol, in *M. venosa* between 1.80 ± 0.03 and 3.30 ±

317   0.07 mmol/mol, in *L. neozelanica* between 1.76 ± 0.04 and 1.79 ± 0.05 mmol/mol, in

318   *G. vitreus* between 1.39 ± 0.04 and 1.99 ± 0.03 mmol/mol and in *N. nigricans*

319   between 1.68 ± 0.06 and 1.94 ± 0.04 mmol/mol.

320

321   *3.2.2. Secondary layer (SL)*

322   *3.2.2.1. Oxygen isotopic compositions*

323   As shown in Figure 5, the oxygen isotopic composition of the fibrous

324   secondary layer of modern brachiopod shells showed a typical pattern towards heavier

325   isotopic composition from the outermost to the innermost part of the shell, reaching a

326   plateau in the innermost regions, as observed by Cusack et al. (2012). This shell layer

327   displays the highest degree of $\delta^{18}O$ variability, particularly in terebratulid brachiopods

328   (up to 5‰), in agreement with previous studies (e.g. Auclair et al., 2003; Yamamoto

329   et al., 2011; Cusack et al., 2012). Generally, no change in the oxygen isotopic

330   composition between central and anterior transects is observed, but some specimens

331   displayed a difference in the variability of $\delta^{18}O$ values between ventral and dorsal

332   valves (e.g. *M. sanguinea,* Fig. 5b). As in Cusack et al. (2012), rhynchonellid

333   brachiopods (*N. nigricans*) record the highest $\delta^{18}O$ at earlier ontogenetic stages than

334   terebratulid brachiopods, resulting in a $\delta^{18}O$ plateau in most of the shell thickness

335   (Fig. 5d).

336     $\delta^{18}O$ values of the secondary layer in the species *T. transversa* range from -2.6

337   ± 0.1‰ in the outermost part to 0.7 ± 0.1‰ in the innermost part in the ventral valve

338   of D500L; from -3.6 ± 0.2‰ to -0.8 ± 0.2‰ in D501L and from -3.8 ± 0.4‰ to 0.2 ±

339   0.4‰ in the ventral valve of D504L. Thus, in *T. transversa*, the overall variability in a

340     $\delta^{18}O$ profile in the secondary layer is between 1.6‰ and 4‰, depending on the

341   specimen and valve studied. In *M. sanguinea*, $\delta^{18}O$ values range from -3.1 ± 0.2‰ to

342   1.3 ± 0.1‰ in DS401L, while it ranges from -2.0 ± 0.2‰ to 2.3 ± 0.4‰ in DS402L,

343   respectively. In DS403L, it ranges between -1.1 ± 0.2‰ and 0.9 ± 0.2‰, and in

344   DS404L between -0.7 ± 0.2‰ and 1.9 ± 0.2‰. The overall variability of $\delta^{18}O$ in a

345   profile of *M. sanguinea* is between 1.8‰ and 4.3‰. $\delta^{18}O$ values of the secondary

346   layer in *C. inconspicua* have an overall variability of 4‰ and range from -1.7 ± 0.4‰

347   to 2.3 ± 0.4‰. In the brachiopod species *M. venosa*, the oxygen isotopic composition

348   of the secondary layer increases as much as 4.3‰ from the outermost towards the

349   innermost regions and ranges between -3.9 ± 0.2‰ and 0.5 ± 0.2‰, in MV05 and

350   from -3.1 ± 0.2‰ to 0.9 ± 0.2‰ in MV17.

351   In *N. nigricans*, oxygen isotopic values of the secondary layer in DS428L

352   range from -0.3 ± 0.4‰ to 1.9 ± 0.4‰. In DS429L, $\delta^{18}O$ values range from -2.1 ±

353   0.2‰ to 2.1 ± 0.3‰ and in DS430L from -0.2 ± 0.2‰ to 2.0 ± 0.2. Thus, in

354   rhynchonellid brachiopods, $\delta^{18}O$ values in the innermost regions are similar between

355   specimens, while the lowest values in the outermost regions could differ up to 2‰.

356     $\delta^{18}O$ variability within a profile is around 2.2‰ in DS428L and DS430L, and 4‰ in

357   DS429L.

358   Although *L. neozelanica* is a three-layered shell, the $\delta^{18}O$ pattern of the

359   secondary layer shows the same trend as for the two-layered shell species, with an

360 increase of $\delta^{18}O$ values from the outermost to the innermost part and a pronounced

361 variability in the secondary layer, from -4.4 ± 0.3‰ in the outermost to -0.3 ± 0.3‰

362 in the innermost part of this shell microstructure (Fig. 5e). In *G. vitreus*, the tertiary

363 layer forms most of the shell thickness (Fig. 5f). Nevertheless, the same trend in the

364 secondary layer is observable in transects performed in the anterior part of the shell

365 (Table 1). $\delta^{18}O$ values in this species are between 0.5 ± 0.2‰ and 1.9 ± 0.2‰ in

366 GV13, between -3.6 ± 0.2‰ and 2.6±0.2‰ in GV47 and range from -0.8 ± 0.2‰ to

367 1.6 ± 0.3‰ in GV78.

368

369 *3.2.2.2. Elemental compositions*

370 The distribution of lithium, sodium and strontium follows a characteristic

371 trend towards lower content from the outermost to the innermost region (Fig. 6). The

372 same trend was described by Perez-Huerta et al. (2008) for magnesium and strontium

373 in the terebratulid brachiopods *T. transversa* and *Terebratulina retusa* (Linnaeus,

374 1758). Li/Ca, Na/Ca and Sr/Ca values reported here are similar to those previously

375 reported for modern brachiopod shells (e.g. Delaney et al., 1989; Lee et al., 2004;

376 Perez-Huerta et al., 2008; Butler et al., 2015; Ullmann et al., 2017; Romanin et al.,

377 2018).

378 In *T. transversa*, Li/Ca values are between 21.5 ± 4.5 and 63.2 ± 4.5

379 µmol/mol, in *M. sanguinea* between 21.2 ± 4.4 µmol/mol and 39.7 ± 5.2 µmol/mol, in

380 *C. inconspicua* between 26.0 ± 4.4 µmol/mol and 29.8 ± 4.5 µmol/mol, in *M. venosa*

381 between 19.2 ± 4.8 and 43.0 ± 5.1 µmol/mol, in *L. neozelanica* between 21.5 ± 5.3

382 and 35.6 ± 5.4 µmol/mol, in *G. vitreus* Li/Ca between 15.2 ± 5.0 µmol/mol and 38.2 ±

383 5.6 µmol/mol and in *N. nigricans* between 27.1 ± 4.5 and 46.3 ± 4.5 µmol/mol.

384   In the secondary layer of *T. transversa*, Na/Ca ratio varies from 3.7 ± 0.1 to

385   11.5 ± 0.3 mmol/mol, in *M. sanguinea* from 6.9 ± 0.1 to 12.4 ± 0.3 mmol/mol, In *C.*

386   *inconspicua* from 8.5 ± 0.2 to 12.0 ± 0.3 mmol/mol, in *M. venosa*, from 7.5 ± 0.2 to

387   13.2 ± 0.2 mmol/mol, in *L. neozelanica* from 6.8 ± 0.2 to 12.1 ± 0.3 mmol/mol, in *G.*

388   *vitreus* from 6.8 ± 0.2 to 12.4 mmol/mol and in the rhynchonellid *N. nigricans* from

389   9.1 ± 0.2 to 14.9 ± 0.3 mmol/mol.

390   Sr/Ca values are between 0.94 ± 0.02 mmol/mol and 1.55 ± 0.04 mmol/mol in

391   *T. transversa*, 1.06 ± 0.02 and 1.54 ± 0.04 mmol/mol in *M. sanguinea*, 1.12 ± 0.02

392   and 1.45 ± 0.04 in *C. inconspicua*, 1.05 ± 0.02 and 2.03 ± 0.07 mmol/mol in *M.*

393   *venosa*, 0.99 ± 0.03 and 1.43 ± 0.04 mmol/mol in *L. neozelanica*, 0.88 ± 0.08 and 1.33

394   ± 0.03 mmol/mol in *G. vitreus* and 0.89 ± 0.04 and 1.50 ± 0.04 mmol/mol in *N.*

395   *nigricans*.

396   In the secondary layer, the Mg/Ca ratio shows the highest variability compared

397   to the other elements measured. Generally, there is a decrease at the boundary

398   between the primary and the secondary layer and then a plateau across the thickness

399   of the secondary layer (Fig. 6h). However, in *T. transversa*, *M. sanguinea* and *C.*

400   *inconspicua*, there is also an increase when reaching the innermost part (Fig. 6g),

401   which is contrary to the trend described by Perez-Huerta et al. (2008). The magnitude

402   of Mg/Ca values agrees with previous studies on modern brachiopod shells (England

403   et al., 2006; Perez-Huerta et al., 2008; Brand et al., 2013; Butler et al., 2015; Ullmann

404   et al., 2017). In *T. transversa*, Mg/Ca values range from 3.7 ± 0.1 to 16.2 ± 0.4

405   mmol/mol, in *M. sanguinea* from 4.5 ± 0.1 to 15.7 ± 0.4 mmol/mol, in *C. inconspicua*

406   from 4.5 ± 0.1 to 11.0 ± 0.3 mmol/mol, in *M. venosa* from 2.2 ± 0.04 to 5.2 ± 0.1, in

407   *L. neozelanica* from 8.0 ± 0.3 to 26.0 ± 0.7 mmol/mol, in *G. vitreus* from 10.2 ± 0.2

408   mmol/mol to 17.1 ± 0.4 and in *N. nigricans* from 8.0 ± 0.2 to 12.9 ± 0.2 mmol/mol.

409

3.2.3. Tertiary layer (TL) (G. vitreus and L. neozelanica)

3.2.3.1. Oxygen isotopic compositions

The tertiary layer has always the highest $\delta^{18}O$ values compared to the oxygen isotopic compositions of the primary and secondary layers. Our values are within the same range of $\delta^{18}O$ values from Romanin et al. (2018) for *L. neozelanica* and *G. vitreus*. Moreover, the $\delta^{18}O$ values are the least variable along the profile, contrary to the variability observed in the secondary layer (Fig. 5e and 5f). For *L. neozelanica*, $\delta^{18}O$ values vary within ≈1‰, from 0.7 ± 0.3‰ to 1.7 ± 0.3‰. In *G. vitreus*, the $\delta^{18}O$ variability depends on the specimen analysed, ranging between 1.2 and 1.8‰. In GV13, $\delta^{18}O$ values are from 1.4 ± 0.2‰ to 3.2 ± 0.2‰, in GV47, from 1.7 ± 0.2‰ to 2.9 ± 0.2‰ and in GV78, from 1.6 ± 0.3‰ to 3.3 ± 0.3‰.

421

3.2.3.2. Elemental ratios

For all the elements measured in the tertiary layer, except Mg, there is a sharp decrease in the values compared to the contents in the primary and secondary layers (Fig. 6), as observed by Romanin et al. (2018) in *G. vitreus*. In the case of Mg/Ca, it is generally depleted, but there are some innermost regions where Mg/Ca increases up to ≈23 mmol/mol (see supplementary Table 2). In this shell fabric, as for the $\delta^{18}O$, the values of all the trace element ratios, except for Mg/Ca, are less variable throughout the profile In *G. vitreus*, Li/Ca values range from 8.6 ± 1.7 to 11.3 ± 1.7 µmol/mol in the ventral valve and from 9.7 ± 1.4 to 16.2 ± 1.5 µmol/mol in the dorsal valve, whereas in *L. neozelanica*, it ranges from 3.9 ± 4.9 to 4.4 ± 4.8 in the ventral valve and from 12.3 ± 3.5 to 14.7 ± 3.6 µmol in the dorsal valve. Na/Ca values are between

433   1.9 ± 0.1 mmol/mol and 4.6 ± 0.1 mmol/mol in *G. vitreus*, while they are between 1.9

434   ± 0.1 and 3.6 ± 0.1 mmol/mol in *L. neozelanica*. Mg/Ca ratio varies from 1.76 ± 0.03

435   mmol/mol to 26.0 ± 0.1 mmol/mol in *G. vitreus* and from 1.7 ± 0.05 mmol/mol and

436   9.0 ± 0.2 mmol/mol in *L. neozelanica*. Sr/Ca values in *G. vitreus* range from 0.55 ±

437   0.01 mmol/mol to 0.74 ± 0.01 mmol/mol and *L. neozelanica* from 0.57 ± 0.01

438   mmol/mol to 0.74 ± 0.01 mmol/mol.

439

440   **4. Discussion**

441

442   *4.1. Isotopic and elemental ratios equilibrium*

443   In order to assess if brachiopod calcite is precipitated in oxygen isotopic

444   equilibrium with surrounding seawater, we calculated the $\delta^{18}O$ equilibrium field using

445   various temperature calibrations ($\delta^{18}O$-T) determined for inorganic calcite, as well as

446   for biogenic carbonates (Epstein et al., 1953; O'Neil et al., 1969; Anderson and

447   Arthur, 1983; Kim and O'Neil, 1997; Brand et al., 2013; Watkins et al., 2013). Then,

448   we compared this equilibrium field with the $\delta^{18}O$ measured in shells for each

449   brachiopod species (Fig. 7). The equilibrium values were calculated using the range of

450   temperature and the $\delta^{18}O_{sw}$ at the site of collection (Table 1) and correcting for Mg

451   concentrations for the equation of Brand et al. (2013). The calibration of Watkins et

452   al. (2013) gives the highest $\delta^{18}O$ equilibrium range, with an enrichment of ≈1.5‰

453   compared to the previously published calibration equations (Epstein et al., 1953;

454   O'Neil et al., 1969; Anderson and Arthur, 1983; Kim and O'Neil, 1997; Brand et al.,

455   2013). The highest $\delta^{18}O$ values, found in the tertiary layer (Fig. 7e,f), are in agreement

456   with the equilibrium range determined from the equation of Watkins et al. (2013) for

457   inorganic calcite. As also found by Ullman et al. (2017) and Bajnai et al. (2018), the

458   equation defined by Watkins et al. (2013) seems to reflect the equilibrium $\delta^{18}O$ values

459   for inorganic calcite much better.

460   To compare the elemental ratios of modern brachiopod shells with equilibrium

461   values for calcite precipitated inorganically, we defined the parameter E_{b-ic}, as

462   follows:

463    $$E_{b-ic} = \frac{D_x}{K_d^x} \qquad (eq.1)$$

464   where D_X is the partition coefficient (the ratio of minor and trace element-

465   MTE/Ca between calcite and seawater) of element X in the brachiopod calcite, and

466   K_d^X is the equilibrium partition coefficient of the same element for calcite precipitated

467   inorganically. K_d^X values were taken from Okumura and Kitano (1986) for Na/Ca

468   (K_d^{Na} = 0.0002), Oomori (1987) for Mg/Ca (K_d^{Mg} = 0.01 at 10°C and 0.015 at 15°C),

469   Marriot et al. (2004) for Li/Ca (K_d^{Li} = 0.0063 at 10°C and 0.0078 at 15°C) and

470   DePaolo (2011) for Sr/Ca (K_d^{Sr} = 0.07). The values were selected since they comply

471   with the temperature at the collection site. By definition, values of E_{b-ic} in equilibrium

472   are equal to one, and if the values are greater or lesser than one, the incorporation of

473   the element is above or below equilibrium, respectively.

474

475   *4.2. The primary layer*

476   As observed in previous studies (e.g. Carpenter and Lohmann, 1995; Auclair

477   et al., 2003; Parkinson et al., 2005; Penman et al., 2013; Rollion-Bard et al., 2016),

478   the primary layer is almost always in oxygen isotopic disequilibrium relative to

479   seawater, with values depleted in ^{18}O (Fig. 5, supplementary Table 1). Based on the

480   correlation between $\delta^{13}C$ and $\delta^{18}O$ values in the primary and secondary layers, this

481   depletion has been ascribed to kinetic fractionation effects (e.g. Carpenter and

482   Lohmann, 1995; Auclair et al., 2003; Parkinson et al., 2005). However, $\delta^{26}Mg$

483   measurements challenged this explanation (Rollion-Bard et al., 2016), because the

484   $\delta^{26}Mg$ values are equivalent between the primary and secondary layers, and close to

485   the magnesium isotopic equilibrium field. It was then suggested that the ^{18}O-depletion

486   could be due to precipitation via amorphous calcium carbonate (ACC) precursors, as

487   proposed by Griesshaber et al. (2009), Cusack et al. (2010), Goetz et al. (2011) and

488   Gaspard and Nouet (2016). ACCs are known to be a precursor phase for the

489   precipitation of calcium carbonate in numerous biogenic carbonates such as the

490   centres of calcification in corals, sea urchins and molluscs (e.g. Hasse et al., 2000;

491   Weiss et al., 2002; Baronnet et al., 2008; Jacob et al., 2008; Vidavsky et al., 2016;

492   Mass et al., 2017). The use of ACC in biominerals as a transient precursor phase is

493   common because this type of calcium carbonate is easily formed and shaped by an

494   organic template (Raz et al., 2002; Weiss, 2003). In the case of the brachiopod

495   primary layer, ACCs seem to be the precursors to the initial formation of crystallites

496   during the production of new calcite fibres (Griesshaber et al., 2009).

497   In the primary layer, all the element data are above equilibrium values (Fig. 6),

498   with an abrupt decrease at the boundary between the primary and the secondary

499   layers. In rhynchonelliform brachiopods, the higher content of Mg/Ca and Sr/Ca in

500   the primary layer is well known (e.g. Cusack and Williams, 2007; England et al.,

501   2006; Perez-Huerta et al., 2008) and has been ascribed to physiological and/or

502   precipitation rate effects. However, as with $\delta^{18}O$ values, the higher element content is

503   likely due to the formation of the primary layer via ACC precursors. The exact

504   pathway of transformation from ACC to calcite or aragonite is still not clear. *In vitro*

505   studies advocate a transformation via dissolution and reprecipitation (Blue et al, 2017;

506 Giuffre et al, 2015; Wolf et al, 2008), whereas *in vivo* observations tend to show a

507 solid-state process via dehydration and rearrangement of the structure (Politi et al,

508 2008; Weiner and Addadi, 2011). These two pathways would likely have different

509 influence on the resulting geochemical signature of the biocarbonates. As there is no

510 consensus yet, we can only speculate on the possible influence of ACC precursors.

511 Many biocarbonates present the same pattern, i.e. finely acicular and

512 microgranular calcite depleted in ^{18}O and ^{13}C, while enriched in some elements. It is,

513 for example, the case for centres of calcification (CoC) in corals (e.g. Adkins et al.,

514 2003; Rollion-Bard et al., 2003, 2010; Meibom et al., 2004; Gagnon et al., 2007;

515 Robinson et al., 2014; Rollion-Bard and Blamart, 2014), primary calcite of

516 foraminifera (e.g. Erez, 2003; Bentov and Erez, 2006; Rollion-Bard et al., 2008) and

517 here primary calcite of brachiopods. Mass et al. (2017) observed that the CoCs are

518 formed via ACC. This transient phase was not yet observed in foraminifera or in

519 brachiopods, but the similitude, both in textural appearance and in geochemical

520 signatures, could be interpreted as the precipitation of primary calcite via ACC. Mg^{2+}

521 is known to be a key ion controlling the stabilization of the ACC by inhibiting the

522 crystallization of $CaCO_3$ (Politi et al., 2009), thus increasing the Mg content

523 (Mavromatis et al., 2017). This agrees with the high Mg content in amorphous phases

524 relative to the aragonite and vaterite found in bivalves (Jacob et al., 2008). In the case

525 of Sr, the uptake has also been shown to be enhanced during ACC transformation, due

526 to the rapid crystal growth during the ACC transformation into calcite crystallites

527 (Littlewood et al., 2017).

528

529 *4.3. The secondary layer*

530   The secondary layer displays the highest variability in $\delta^{18}O$ values (up to 5‰)

531   and in elemental ratios. In all the specimens investigated, there is a common trend for

532     $\delta^{18}O$ and elemental ratios, reaching a plateau termed "equilibrium zone" by Perez-

533   Huerta et al. (2008), in the innermost part of the secondary layer. Here, we will use

534   the term "plateau zone" to refer to this stable geochemical part of the secondary layer,

535   to avoid the perception that the precipitation is in isotopic or elemental equilibrium.

536   The common pattern and the high variability concerning the geochemical

537   composition of the secondary layer cannot be only explained by variations of the

538   external environmental parameters, (e.g. temperature and salinity). For example, the

539   annual average temperature range at the site of collection is 4°C for *T. transversa*,

540   6°C for *M. sanguinea*, *C. inconspicua* and *N. nigricans* and 3.5°C for *M. venosa*, and

541   thus can only explain a $\delta^{18}O$ variation between 0.8 and 1.3‰, considering a $\delta^{18}O$-T

542   dependence of -0.22‰/°C (Epstein et al., 1953). The $\delta^{18}O$ variation due to salinity

543   change according to the $\delta^{18}O$-salinity relationship established by Gillikin et al (2005)

544   for Pudget Sound and by Delaygue et al (2000) for the other collecting sites, leads to a

545   variation of 0.3‰ for *T. transversa*, 1.6‰ for *M. sanguinea*, *C. inconspicua* and *N.*

546   *nigricans* and of 0.1‰ for *M. venosa*. Consequently, the geochemical variability of

547   the secondary layer must be explained by some additional physiological effects

548   controlling the $\delta^{18}O$ and elemental composition of the brachiopod secondary layer.

549   The possible causes could be: (1) Rayleigh fractionation, (2) variation of pH of the

550   fluid of calcification and (3) kinetic effects.

551   (1) Rayleigh fractionation has been proposed to explain the variability of

552   different elemental ratios in biocarbonates as foraminifera and corals (Elderfield et al.,

553   1996; Cohen et al., 2006; Gagnon et al., 2007). As we observe in the Figure 8, there is

554   a covariation between Sr/Ca and Na/Ca, which could be caused by Rayleigh

555   fractionation. To test this hypothesis, we performed a theoretical Rayleigh

556   fractionation model. For this, we chose the example of *T. transversa* measurements

557   for Sr/Ca and Na/Ca ratios (Fig. S3), as it is the species with the highest number of

558   analyses. Four possible scenarios were investigated. In the scenario (i), the initial fluid

559   has Na/Ca and Sr/Ca content similar to that of seawater, i.e. Na/Ca = 45.9 mol/mol

560   and Sr/Ca = 8.6 mmol/mol, and partition coefficients of inorganic calcite (D_{Na} =

561   0.0002, Okumura and Kitano, 1986; and D_{Sr} = 0.07, DePaolo, 2011). In the scenario

562   (ii), the initial fluid is the seawater, but the partition coefficients are calculated to have

563   the same initial element content as in brachiopod calcite (D_{Na} = 0.00011 and D_{Sr} =

564   0.11). In scenario (iii), partition coefficients are those for inorganic calcite, but the

565   trend is estimated adjusting the elemental ratios of the initial fluid (Na/Ca = 32

566   mol/mol and Sr/Ca = 12 mmol/mol). Applying the equation of Elderfield et al. (1996)

567   for Rayleigh-type incorporation of elements, we observe that none of these scenarios

568   reproduce the trend found in the brachiopod secondary layer (Fig. S3). To have the

569   'Best fit' parameters to reproduce our trend, we applied in the scenario (iv) the

570   method of Gagnon et al. (2007) by combining Na/Ca and Sr/Ca with the following

571   equation:

572
$$\ln\left(\frac{Sr}{Ca}\right) = \left(\frac{D_{Sr}-1}{D_{Na}-1}\right)\ln\left(\frac{Na}{Ca}\right) + \left[\ln\left(\frac{Sr}{Ca}\right)_0 - \left(\frac{D_{Sr}-1}{D_{Na}-1}\right)\ln\left(\frac{Na}{Ca}\right)_0\right] \qquad (eq.\,2)$$

573   As in Rollion-Bard and Blamart (2015), we calculate D_{Sr} from the slope of the

574   log-log plot of the Sr/Ca-Na/Ca relationship (slope=0.37). Using D_{Na} calculated from

575   the lowest brachiopod Na/Ca value (Na/Ca=5.01mmol/mol, D_{Na}=0.00011) and

576   assuming that the fluid Na/Ca ratio is equivalent to seawater, it gives a value of

577   D_{Sr}=0.63, which is 9 times higher than D_{Sr} of inorganic calcite, i.e. D_{Sr}=0.07. With

578   D_{Na}=0.00011, Na/Ca$_{sw}$=45.9 mol/mol and the calculated D_{Sr}=0.63, Sr/Ca of the

579   precipitating fluid is 1.48 mmol/mol. In this case, if Na/Ca is similar to seawater, then

580 Sr/Ca of the calcifying fluid is very different from seawater, in the order of six times

581 lower. In conclusion, Rayleigh fractionation is unlikely to be the mechanism

582 responsible of the MTE and $\delta^{18}O$ variations in the secondary layer calcite.

583   (2) The pH can control the isotopic composition of oxygen during the

584 precipitation of calcium carbonate (e.g. McCrea, 1950; Usdowski et al., 1991

585 Usdowski and Hoefs, 1993; Zeebe, 1999, 2001, 2007). The relative proportions of the

586 three dissolved carbonate species (H_2CO_3, HCO_3^-, CO_3^{2-}) depend on the solution pH.

587 As these carbonate species have different $\delta^{18}O$ values (Usdowski and Hoefs, 1993;

588 Kim and O'Neil, 1997; Zeebe and Wolf-Gladrow, 2001; Beck et al., 2005), it is

589 assumed that the $\delta^{18}O$ value of carbonate can be dependent of pH via the proportional

590 incorporation of the different carbonate species. Internal pH has been determined by

591 microelectrode measurements with the resulting value of ~ 7.8 (Jurikova et al., 2019).

592 Another way to access this parameter is the measurements of $\delta^{11}B$, as $\delta^{11}B$ of

593 carbonates is a pH proxy (e.g. Vengosh et al., 1991; Hemming and Hanson, 1992).

594 Penman et al. (2013) analysed the boron and oxygen isotopic compositions in the

595 brachiopod shells of *T. transversa* and *M. venosa*. In *T. transversa*, a variability of

596 1.25‰ in $\delta^{18}O$ corresponds to a variability of 2‰ in $\delta^{11}B$, from 16.51‰ to 18.50 ‰.

597 This variability in $\delta^{11}B$ values in *T. transversa* corresponds to a pH variation of 0.2

598 pH-units (from a pH of 8.10 to 8.30, using a pK_B of 8.82, and $\delta^{11}B_{sw}$=39.61‰;

599 Dickson, 1990; Millero, 1995; Foster et al., 2010). In *M. venosa*, there is essentially

600 no $\delta^{18}O$ variation (from 2.56 ‰ to 2.53 ‰), but the $\delta^{11}B$ values change by 2.85‰,

601 from 14.76‰ to 17.61‰, corresponding to a pH variation of 0.3 pH-unit (pH from

602 7.86 to 8.16). For this brachiopod, the $\delta^{11}B$ variability combined with the stability of

603 $\delta^{18}O$ signal is indicative that pH changes have occurred within the shell but did not

604 lead to differences in the oxygen isotopic composition. Therefore, changes in the

605   internal pH seem not responsible for the variation in the oxygen isotopic composition

606   of the secondary layer of modern brachiopod shells.

607   Changes on the incorporation of elements throughout the secondary shell layer

608   due to pH are also unlikely. In Penman et al. (2013), it is shown that the highest

609   values of $\delta^{11}B$ are in the mid-part of the secondary layer, corresponding to the highest

610   pH of 8.16, while in the outermost and innermost secondary layers a drop in $\delta^{11}B$

611   occurs indicating lower pH values down to 7.86. So pH does not covary with the trend

612   of elemental ratios in the secondary layer (Fig S4). This assumption, however, has to

613   be verified by measuring both $\delta^{11}B$ and elements by *in situ* techniques. In the case of

614   Na/Ca and Mg/Ca, this is also supported by inorganic calcite experiments, where the

615   uptake of Na/Ca and Mg/Ca is independent of pH in the range of pH 7.38-10.60 and

616   6.8-9, respectively (Ishikawa and Ichikuni, 1984; Hartley and Mucci, 1996). Although

617   we do not observe any trend concerning pH and Mg/Ca, the assertion that Mg/Ca is

618   independent on the pH has to be taken carefully, because in Mavromatis et al. (2013),

619   the Mg/Ca ratio is dependent on the saturation state (Ω), a parameter that is directly

620   related to the pH of the solution.

621   (3) Kinetic effects are often thought to cause the depletion in ^{18}O of the

622   precipitated carbonate (McConnaughey, 1989a,b; McConnaughey et al., 1997; Zeebe

623   and Wolf-Gladrow, 2001; Auclair et al., 2003; Rollion-Bard et al., 2003, 2011). They

624   occur because during the CO_2 hydration and hydroxylation reactions, the bicarbonate

625   ions do not have the time to equilibrate with H_2O in the calcifying fluid. Even if the

626   link between the calcification rate and the growth rate is not straightforward, it seems

627   that the magnitude of the kinetic fractionation effect changes during brachiopod

628   lifetime. Brachiopod shells grow from the posterior towards the anterior part and from

629   the exterior towards the interior (Ye et al., 2018), having its highest growth rates at

630   the early stages of their life (e.g. Paine, 1969; Auclair et al., 2003; Yamamoto et al.,

631   2013). This implies that fibres from the posterior and outermost secondary layer were

632   precipitated when the brachiopod was at its juvenile stage showing rapid growth. This

633   part corresponds to the highest depletion in ^{18}O relative to equilibrium (Fig. 5), as

634   expected from theoretical kinetic consideration (McConnaughey, 1989a; Zeebe and

635   Wolf-Gladrow, 2001; Auclair et al., 2003; Rollion-Bard et al., 2003, 2011). The same

636   holds for the calcite fibres of the innermost and anterior regions, which were

637   deposited in the most mature stages of the brachiopod life with slow growth rates

638   (Paine, 1969; Auclair et al., 2003; Ye et al., 2018) and thereby are less affected by

639   kinetic fractionation effects.

640   The overall profile of lithium, sodium and strontium distribution in the

641   secondary layer can also be explained by kinetic effects. The higher element content

642   in calcite due to kinetics has been theoretically explained by different mechanisms,

643   such as the growth entrapment model, surface reaction model or the ion-by-ion model

644   (Watson and Liang, 1995; Watson, 2004; DePaolo, 2011; Nielsen et al., 2012). Many

645   experiments of inorganic calcite precipitated under controlled conditions showed that

646   Sr/Ca ratios are dependent on calcification rates (i.e. Morse and Bender, 1990;

647   Gabitov and Watson, 2006; Tang et al., 2008; Gabitov et al., 2014; Alkhatib and

648   Eisenhauer, 2017). As $D_{Sr}<1$ in calcite, the Sr/Ca ratio increases with calcification

649   rates (Mavromatis et al., 2013). This is also the case for the incorporation of Na^+ into

650   calcite in the laboratory experiment carried out by Busenberg and Plummer (1985).

651   As the shell becomes more mature and precipitates calcite at slower rates in the

652   innermost and anterior regions of the shells (Paine, 1969; Auclair et al., 2003), like

653   with the oxygen isotopic composition, the Na/Ca and Sr/Ca ratios decrease until

654   reaching the "plateau zone" in the innermost region. The fact that Sr/Ca is correlated

655 with Na/Ca and the oxygen isotopic compositions in the secondary layer (Fig. 8)

656 highlights once more the control of calcification rate on $\delta^{18}O$ values, Na/Ca and Sr/Ca

657 in the secondary layer of terebratulid brachiopods.

658   Lithium incorporation is positively correlated with calcification rates in

659 aragonite precipitated inorganically (Gabitov et al., 2011). However, there is no study

660 yet addressing the dependence between lithium incorporation and calcification rates

661 into calcite, but if we assume the same dependence between calcite and aragonite,

662 then the trend towards lower lithium content in the innermost regions can also be

663 explained by kinetic effects.

664   Finally, since brachiopod species studied here precipitate low-Mg calcite

665 shells (Lowenstam and Weiner, 1989), we can expect that $E_{b\text{-}ic}$ values for magnesium

666 are below 1. It is, indeed, the case because $E_{b\text{-}ic(Mg)}$ is between 0.05 to 0.2 (Fig. 6),

667 indicating that they incorporate five to twenty times less magnesium than calcite in

668 equilibrium with ambient seawater. This is likely because of a physiological

669 mechanism of Mg exclusion (Lowenstam, 1961; Lowenstam and Weiner, 1989;

670 England et al., 2006; Perez-Huerta et al., 2008), as already observed in other

671 calcifying organisms like foraminifera and bivalves (e.g. Lorens and Bender, 1977;

672 Lea et al., 1999; Erez, 2003). The exclusion of Mg is probably due to its inhibition

673 role on the nucleation and growth of calcite (i.e. Lippmann, 1973; Mucci and Morse,

674 1983; Zhang and Dave, 2000). Moreover, we did not observe a trend towards lower

675 values in the innermost regions, in contrast to the other elements, probably due to the

676 strong biological control that the brachiopod exerts on this element.

677

678 *4.4 Tertiary layer*

679

680   The tertiary layer has the highest $\delta^{18}O$ values and the smallest overall

681   variability compared to the other layers. The $\delta^{18}O$ variations are in the order of 1‰ to

682   1.5‰, in agreement with the temperature and salinity variation at the sites of

683   collection. Moreover, this layer is within the equilibrium field of inorganic calcite

684   using the equation of Watkins et al. (2013).

685   In the tertiary layer, we observe a strong depletion in Li/Ca, Na/Ca and Sr/Ca

686   ratios relative to the primary and secondary layers. Grossman et al. (1996) also found

687   the same depletion pattern in elements in the tertiary layer of Pennsylvanian fossil

688   brachiopod shells (*Crurithyris planoconvexa*, *Composita subtilita*, *Neospirifer*

689   *dunbari* and *Neospirifer pattersoni*). The $E_{b\text{-}ic.}$ values are two times lower than in the

690   secondary layer, ranging between 0.25 to 1.02 for Li/Ca, between 0.21 and 0.39 for

691   Na/Ca and between 0.86 and 1.29 for Sr/Ca, depending on the brachiopod species.

692   The lower element content in the tertiary layer can be explained by two scenarios.

693   First, the differences in element contents between the secondary and tertiary

694   layers can be due to contamination by organic matter. The secondary layer has higher

695   organic content than the tertiary layer (MacKinnon and Williams, 1974; Goetz et al.,

696   2009; Ye et al., 2018). As Ca is a trace component in organic matter, any

697   contamination should be detected in the signal intensity detected by the ICP-MS by a

698   decrease in the number of counts of ^{43}Ca. As the calcium signal intensity was at the

699   same level for all the measurements, it is likely that organics do not affect the content

700   of elements in the secondary layer.

701   Second, it can reflect that either the partition coefficients of inorganic calcite

702   are not well constrained, or that there is different fractionation for elements during the

703   ionic transport through the cell membranes between shell microstructures. To our

704   knowledge, there is only one study available for Na and Li incorporation into

705   synthetic calcite (Okumura and Kitano, 1986; Marriott et al., 2004, respectively),

706   while the incorporation of Sr into calcite has been extensively studied (i.e. Lorens,

707   1981; Gabitov and Watson, 2006; Tang et al., 2008; Alkhatib and Eisenhauer, 2017).

708   When comparing Li/Ca, Na/Ca and Sr/Ca with inorganic calcite, we observe that Li,

709   Na and Sr in brachiopod calcite goes towards equilibrium values in the innermost

710   regions of the secondary layer, and therefore, we assume that the innermost regions of

711   the secondary layer are the portions in equilibrium with ambient seawater. Therefore,

712   if the values of the partition coefficients are not the cause, it must be another

713   mechanism accounting for the depletion of elements in the tertiary layer. The tertiary

714   layer is produced when the organics that enclose the secondary layer fibres are not

715   produced anymore, so the fibres lose their boundaries and coalesce into the tertiary

716   layer prisms (MacKinnon and Williams, 1974; Williams, 1997). Therefore, this

717   change in the secretory regime of the outer epithelial cells probably produces different

718   fractionation of elements during the ionic transport through the cell membranes,

719   leading to the depletion of elements in the tertiary layer.

720

721   *4.5. Elemental ratios: environmentally controlled?*

722   The possible control of environmental parameters (temperature, salinity and

723   pH) on the partition coefficients of Li, Na, Mg and Sr in the "plateau zone" secondary

724   layer, i.e. innermost region, of terebratulid brachiopods is shown in Figure 9. Data

725   relative to the significant ($p < 0.05$) linear relationships and statistics are given in Table

726   4. The relationships account only for the element values in the innermost secondary

727   layer, i.e., the "plateau zone", because we assume this is the region the closest to

728   equilibrium with ambient seawater or fluid of calcification (Fig. 6).

729   As proposed by Perez-Huerta et al. (2008) for the incorporation of Mg and Sr,

730   differences in $E_{b-ic.}$ between Mg/Ca and Sr/Ca in the "plateau zone" could be due to

731   physiological control on the incorporation of elements. This is particularly evident for

732   Mg/Ca ratios. Their relatively low values are probably due to the exclusion of Mg

733   from the fluid of calcification via biological mechanism(s) like Mg^{2+}/Na^+ antiporters

734   or Mg^{2+}-ATPase (e.g. Zeebe and Sanyal, 2002). However, the exclusion of Mg

735   apparently does not restrict the use of Mg in biogenic carbonates: foraminifera also

736   exclude Mg and are extensively used to reconstruct paleotemperatures on the basis of

737   species-specific calibrations (e.g. Nürnberg et al., 1996; Rosenthal et al., 2011; Evans

738   et al., 2015). Therefore, whether Mg/Ca reliably records temperatures or not has been

739   a matter of debate; in some studies they defend its potential use (e.g. Brand et al.,

740   2003; Butler et al., 2015), while others discourage it (Lowenstam, 1961; Perez-Huerta

741   et al., 2008), arguing in favour of the strong biological control of Mg in low-Mg

742   calcifying brachiopods superimposing the environmental parameters. In the Figure 9g,

743   we observe that D_{Mg} increases with temperature. This relationship is statistically

744   significant ($p < 0.05$, Table 4) and in agreement with inorganic calcite experiments

745   (Oomori et al., 1987). Nevertheless, when comparing with other values from the

746   literature (Delaney et al., 1989; Perez-Huerta et al., 2008; Brand et al, 2013; Butler et

747   al., 2015), there is no apparent trend. The latter could be due to different sampling

748   techniques. Here, we consider only the values of the "plateau zone" only, while in

749   other studies, Mg/Ca is the bulk value or the average of the entire secondary layer.

750   The same holds for salinity. D_{Mg} increases with salinity, this relationship being

751   statistically significant ($p < 0.05$, Table 4), if only our data are considered. With

752   previous published values, the data become scattered. In consequence, we observe a

753   trend of D_{Mg} with temperature and salinity, supporting its potential use as proxies, but

754   this assertion is complicated due to the different sampling techniques, emphasizing

755   that an appropriate and careful sampling is critical.

756   In inorganic calcite, D_{Sr} changes with temperature: Sr/Ca increases by 1%

757   with 1°C increase, at least between 16 and 27°C (Gabitov and Watson, 2006).

758   However, we do not observe any relation between D_{Sr} of the plateau of the secondary

759   layer and temperature, similarly as in previously published studies (Lowenstam, 1961;

760   Perez-Huerta et al., 2008; Ullmann et al., 2017). Likewise, there is no relation

761   between Sr/Ca and pH and salinity (Fig. 9j, 9k, 9l). As mentioned before, this could

762   be due to different sampling techniques. Lowenstam (1961), however, suggested the

763   use of Sr/Ca of brachiopod calcite as temperature recorder instead of Mg/Ca. This

764   suggestion was based on the assumption that Sr is not as strongly controlled by the

765   physiology of the organism as Mg/Ca. In view of our data, the Sr/Ca ratio of the

766   secondary layer does not seem to be a suitable proxy for seawater temperature.

767   Regarding D_{Li}, there is a negative relationship with temperature (Fig. 9a), with

768   a decrease of D_{Li} by 3% per degree Celsius. The relation between D_{Li} and temperature

769   is in agreement with the study of Delaney et al. (1989) and Dellinger et al (2018) on

770   modern brachiopods. Marriott et al. (2004) observed the same effect for inorganic

771   calcite, despite a constant offset between brachiopod and inorganic calcite. The cause

772   of this offset is not determined yet.

773   Finally, for D_{Na}, there is a relationship with salinity, which is statistically

774   significant ($p < 0.05$, Table 4, Fig. 9f). The correlation of D_{Na} with salinity in

775   brachiopod calcite is in agreement with studies investigating the relationship between

776   Na/Ca and salinity in both, inorganically precipitated calcium carbonate experiments

777 (Kitano et al., 1975; Ishikawa and Ichikuni, 1984; Okumura and Kitano, 1986) and

778 marine calcifying organisms such as foraminifera (Wit et al., 2013), oysters (Rucker

779 and Valentine, 1961) and barnacle shells (Gordon et al., 1970). Then, if Na/Ca of the

780 "plateau zone" of the brachiopod calcite is primarily controlled by salinity, it opens

781 the possibility of using this ratio as a proxy for seawater salinity, knowing the secular

782 variations of Na/Ca in seawater. D_{Na} also co-varies with temperature, but not with pH,

783 which is in agreement with the findings of Ishikawa and Ichikuni (1984). Therefore,

784 to decipher the control of D_{Na} by these two environmental parameters, we suggest its

785 use in combination to another temperature proxies such as Li/Ca ratios.

786

787 *4.6 Implications for the use of brachiopod geochemical data as paleoenvironmental*

788 *proxies.*

789   This study is the first investigating both the oxygen isotopic composition and

790 element content at the microstructural level by using high spatial resolution in situ

791 techniques. This allowed us to study the $\delta^{18}O$ and elemental ratios in the different

792 shell fabrics: primary, secondary and tertiary layers.

793   The use of two-layered shells as archives of geochemical proxies has to be

794 cautiously done. As it was already demonstrated by previous studies (e.g. Carpenter

795 and Lohmann, 1995; Auclair et al., 2003; Cusack et al., 2012; Romanin et al., 2018),

796 the best part to use is the innermost secondary layer. However, this "plateau zone" has

797 not always the same thickness between species (Fig. 5), and it could be difficult to

798 determine the exact zone to analyse. In this context, as proposed by Cusack et al.

799 (2012), rhynchonellid brachiopods are more reliable because of their larger "plateau

800 zone" than terebratulid brachiopods. This implies that the majority of their secondary

801 layer can be used as proxy in paleoenvironmental studies. Moreover, as the $\delta^{18}O$

802   values of the secondary layer, even in the "plateau zone" are not always in isotopic

803   equilibrium with seawater, a specific calibration curve for brachiopod has to be

804   defined and used, as proposed by Brand et al (2013).

805   The tertiary layer as a reliable proxy is an important finding for its use in

806   paleotemperature reconstructions. Several fossil brachiopods have a tertiary layer, like

807   the classes Rhynchonellata and Strophomenata, (Williams, 1968), which dominated

808   the Paleozoic seas (e.g. Curry and Brunton, 2007). The tertiary layer is likely to be

809   better preserved than the secondary layer because the columns of this layer are

810   morphologically more stable and depleted in magnesium relative to the secondary

811   layer. Some Carboniferous genera, like those of the Gigantoproductinae, developed

812   shells with a very thick tertiary layer, exceeding 1cm (Angiolini et al., 2012). This

813   tertiary layer has a maximum $\delta^{18}O$ variation in the well-preserved – not diagenetically

814   altered - parts of 1.1‰, agreeing with possible annual temperature variations. In

815   addition, Grossman et al. (1996) found a depletion of sodium and magnesium in the

816   tertiary layer of fossil brachiopods, with up to three times less content compared to

817   the secondary layer. These findings are in agreement with our measurements in

818   modern brachiopods. Thus, the biomineralization processes of the tertiary layer seem

819   consistent between fossil and modern specimens. Consequently, when three-layered

820   shells are available, the most suitable shell fabric to use for reconstructions of

821   seawater temperature from $\delta^{18}O$ values is the tertiary layer.

822   The depletion of elements in the tertiary layer compared to the primary and

823   secondary layers may have implications on the analysis of the isotopic composition of

824   various trace elements, as δ^7Li and $\delta^{11}B$. For example, Li is about two to four times

825   less concentrated in the tertiary layer (Fig. 6) than in the secondary layer, involving

826   the need to use more material for isotopic analyses. This depletion in elements,

827 however, should not be interpreted as diagenetic effects, differences in precipitation

828 or change in Li concentration of seawater. As an example, in Delaney et al. (1989),

829 the spiriferid species *Martinia* sp. and *Choristites* sp., respectively from the Permian

830 and Carboniferous, are depleted in Li/Ca, with values as low as 3.5 µmol/mol in

831 *Martinia* sp. and 1.4 µmol/mol in *Choristites* sp. The Sr/Ca ratio analysed by Popp et

832 al. (1986) from the same taxa is of around 0.5 to 1 mmol/mol and 0.3 to 1.2

833 mmol/mol in *Martinia* sp. and *Choristites* sp, respectively. Species of *Martinia* are

834 known to precipitate a tertiary layer (Angiolini, 2001), and analysis of the shell

835 microstructure of *Choristites mosquensis* from the Pennsylvanian of Iran (Berra et al.,

836 2017) has revealed the occurrence of a thick tertiary layer (L. Angiolini, pers. com.).

837 The depletion of both Li/Ca and Sr/Ca is in agreement with our findings on the

838 tertiary layer on modern brachiopods, and the presence of a tertiary layer could

839 explain the reason for the very low values measured in these fossil brachiopod

840 species.

841

842 **5. Conclusions**

843

844 1. The primary layer of modern brachiopods is in oxygen isotopic and element

845   disequilibrium. The primary layer is depleted in ^{18}O and globally enriched in

846   MTE, possibly due to the precipitation via amorphous calcium carbonate

847   (ACC) precursors.

848 2. In the secondary layer, we observed a general trend towards equilibrium or

849   near equilibrium values due to kinetic fractionation effects, for both δ^{18}O

850   values and element content (except for Mg/Ca). The outer secondary layer is

851   more affected by kinetic fractionation processes and thus out of equilibrium,

852   whereas in the innermost regions, that are no or very little affected,
853   equilibrium can be achieved.

854   3. The tertiary layer has $\delta^{18}O$ values in the range of equilibrium values and
855   records the temperature variation at the sampling location. This shell layer is
856   likely precipitated at slower growth rates, and not affected by kinetic effects.
857   Consequently, the tertiary layer seems the most suitable shell microstructure to
858   use for temperature reconstructions, if present. However, it is depleted in all
859   the elements studied here, hampering their use in studies of non-traditional
860   isotopic systems.

861   4. A correlation between Na/Ca, Sr/Ca ratios and $\delta^{18}O$ is recorded in the
862   secondary layer of modern brachiopod species probably due to kinetic
863   fractionation effects. This relationship may have a potential application to
864   track kinetic effects in fossil organisms (Ullman et al., 2017).

865   5. The Mg/Ca ratios are highly variable within the shell. They are always below
866   expected equilibrium values due to physiological exclusion processes. We
867   observe a trend with environmental parameters like temperature and salinity,
868   but not when other published Mg/Ca values in modern brachiopods are
869   considered. Consequently, the use of Mg/Ca of brachiopod shells as proxy for
870   temperature needs further evaluation.

871   6. A trend of D_{Li} with temperature, and a trend of D_{Na} with temperature and
872   salinity are found for the "plateau zone" of the secondary layer. Further
873   investigation of their potential use as temperature and salinity proxies is
874   required before any application for paleoreconstructions.

875

886   **References**

887   Adkins, J. F., Boyle, E. A., Curry, W. B., Lutringer, A., 2003. Stable isotopes in deep-

888   sea corals and a new mechanism for "vital effects." Geochim. Cosmochim. Acta

889   67(6), 1129–1143. https://doi.org/10.1016/S0016-7037(02)01203-6

890   Alkhatib, M., Eisenhauer, A., 2017. Calcium and Strontium Isotope Fractionation in

891   Aqueous Solutions as a Function of Temperature and Reaction Rate; I. Calcite.

892   Geochim.   Cosmochim.   Acta   209,   296–319.

893   https://doi.org/10.1016/j.gca.2016.09.035

894   Anderson T. F., Arthur M.A., 1983. Stable isotopes of oxygen and carbon and their

895   application to sedimentologic and paleoenvironmental problems. In: Arthur

896   M.A., Anderson T.F., Kaplan I.R., Veizer J. & Land L.S. (Eds.), Stable Isotopes

897   in Sedimentary Geology. Short Course Notes No. 10. Society of Economic

898   Paleontologist   and   Mineralogists,   Tulsa,   Oklahoma,   pp.   1–151.

899   https://doi.org/10.2110/scn.83.01.0000

900   Angiolini, L., 2001. Permian brachiopods from Karakorum (Pakistan). Pt. 3. Riv. Ital.

901   Paleontol. S. 107 (3), 307–344. https://doi.org/10.13130/2039-4942/5438

902   Angiolini L., Jadoul F., Leng M.J., Stephenson M.H., Rushton J., Chenery S., Crippa

903   G., 2009. How cold were the Early Permian glacial tropics? Testing sea surface

904   temperature using the oxygen isotope composition of rigorously screened

905   brachiopod shells. J. Geol. Soc. 166, 933–945. https://doi.org/10.1144/0016-

906   76492008-096R

907   Angiolini, L., Stephenson, M.H., Leng, M.J., Jadoul, F., Millward, D., Aldridge, A.,

908   Andrews, J.E., Chenery, S., Williams, G., 2012. Heterogeneity, cyclicity and

909   diagenesis in a Mississippian brachiopod shell of palaeoequatorial Britain. Terra

910   Nova 24, 16–26. https://doi.org/10.1111/j.1365-3121.2011.01032.x

911   Auclair A. C., Joachimski M. M., Lécuyer C., 2003. Deciphering kinetic, metabolic

912   and environmental controls on stable isotope fractionations between seawater

913   and the shell of *Terebratalia transversa* (Brachiopoda). Chem. Geol. 202(1),

914   59–78. https://doi.org/10.1016/S0009-2541(03)00233-X

915   Bajnai, D., Fiebig, J., Tomašových, A., Milner Garcia, S., Rollion-Bard, C., Raddatz,

916   J., Löffler, N., Primo-Ramos, C., Brand, U., 2018. Assessing kinetic

917   fractionation in brachiopod calcite using clumped isotopes. Sci. Rep. 8, 533.

918   https://doi.org/10.1038/s41598-017-17353-7

919   Barker S., Greaves M., Elderfield H., 2003. A study of cleaning procedures used for

920   foraminiferal Mg/Ca paleothermometry. Geochem. Geophy. Geosy. 4, 8407.

921   https://doi.org/10.1029/2003GC000559

922   Baronnet, A., Cuif, J.-P., Dauphin, Y., Farre, B., Nouet, J., 2008. Crystallization of

923   biogenic Ca-carbonate with organo-mineral micro-domains. Structure of the

924   calcite prisms of the Pelecypod *Pinctada margaritifera* (Mollusca) at the

925   submicron to nanometre ranges. Mineral. Mag. 72, 617–626.

926   https://doi.org/10.1180/minmag.2008.072.2.617

927   Bates, N.R., Brand, U., 1991. Environmental and physiological influences on isotopic

928   and elemental compositions of brachiopod shell calcite: implications for the

929   isotopic evolution of Paleozoic oceans. Chem. Geol. Isot. Geosci. Sect. 94, 67–

930   78. https://doi.org/10.1016/S0009-2541(10)80018-X

931   Beck, W.C., Grossman, E.L., Morse, J.W., 2005. Experimental studies of oxygen

932   isotope fractionation in the carbonic acid system at 15°, 25°, and 40 °C.

933   Geochim. Cosmochim. Acta 69, 3493–3503.

934   https://doi.org/10.1016/j.gca.2005.02.003

935   Bentov S., Erez J., 2006. Impact of biomineralization processes on the Mg content of

936   foraminiferal shells: a biological perspective. Geochem. Geophys. Geosyst. 7,

937   Q01P08. https://doi.org/10.1029/2005GC001015.

938   Berra, F., Zanchi, A., Angiolini, L., Vachard, D., Vezzoli, G., Zanchetta, S., Bergomi,

939   M., Javadi, H. R., Kouhpeyma, M., 2017. The upper Palaeozoic Godar-e-Siah

940   Complex of Jandaq: Evidence and significance of a North Palaeotethyan

941   succession in Central Iran. J. Asian Earth Sci. 138, 272–290.

942   https://doi.org/10.1016/j.jseaes.2017.02.006

943   Blue, C.R., Giuffre, A., Mergelsberg, S., Han, N., De Yoreo, J.J., Dove, P.M., 2017.

944   Chemical and physical controls on the transformation of amorphous calcium

945   carbonate into crystalline $CaCO_3$ polymorphs. Geochim Cosmochim Acta 196,

946   179-196.

947   Brand, U., 1989. Biogeochemistry of Late Paleozoic North American brachiopods and

948   secular variation of seawater composition. Biogeochemistry 7, 159–193.

949   https://doi.org/10.1007/BF00004216

950   Brand, U., Veizer, J., 1980, Chemical diagenesis of a multi-component carbonate

951   system - 1. Trace elements. J. Sediment. Petrol. 50, 1219–1236.

952   https://doi.org/10.1306/212F7BB7-2B24-11D7-8648000102C186

953   Brand U., Logan A., Hiller N., Richardson J., 2003. Geochemistry of modern

954   brachiopods: applications and implications for oceanography and

955   paleoceanography. Chem. Geol. 198, 305–334. https://doi.org/10.1016/S0009-

956   2541(03)00032-9

957   Brand U., Logan A., Bitner M.A., Griesshaber E., Azmy K., Buhl D., 2011. What is

958   the ideal proxy of Paleozoic seawater chemistry? Australas. Palaeontolol. Mem.

959   41, 9–24.

960   Brand U., Azmy K., Bitner M. A., Logan A., Zuschin M., Came R., Ruggiero E.,

961   2013. Oxygen isotopes and $MgCO_3$ in brachiopod calcite and a new

962   paleotemperature   equation.   Chem.   Geol.   359,   23–31.

963   https://doi.org/10.1016/j.chemgeo.2013.09.014

964   Brand, U., Azmy, K., Griesshaber, E., Bitner, M. A., Logan, A., Zuschin, M.,

965   Ruggiero, E., Colin, P.L., 2015. Carbon isotope composition in modern

966   brachiopod calcite: A case of equilibrium with seawater?. Chem Geol 411, 81-

967   96.

968   Buening, N., Carlson, S.J., 1992, Geochemical investigation of growth in selected

969   Recent   articulate   brachiopods.   Lethaia   25,   331–345.

970   https://doi.org/10.1111/j.1502-3931.1992.tb01402.x

971   Buening, N., Spero, H.J., 1996. Oxygen- and carbon-isotope analyses of the articulate

972   brachiopod *Laqueus californianus*. A recorder of environmental changes in the

973   subeuphotic   zone.   Mar.   Biol.   127,   105–114.

974   https://doi.org/10.1007/BF00993650

975   Busenberg, E., Plummer, L.N., 1985. Kinetic and thermodynamic factors controlling

976   the distribution of SO_4^{2-} and Na^+ in calcites and selected aragonites. Geochim.

977   Cosmochim. Acta 49, 713–725. https://doi.org/10.1016/0016-7037(85)90166-8

978   Butler S., Bailey T.R., Lear C.H., Curry G.B., Chems L., McDonald, I., 2015. The

979   Mg/Ca temperature relationship in brachiopod shells: Calibrating a potential

980   palaeoseasonality   proxy.   Chem.   Geol.   397,   106–117.

981   https://doi.org/10.1016/j.chemgeo.2015.01.009

982   Carpenter S. J., Lohmann K. C., 1995. $\delta^{18}O$ and $\delta^{13}C$ values of modern brachiopod

983   shells. Geochim.   Cosmochim.   Acta 59(18),   3749–3764.

984   https://doi.org/10.1016/0016-7037(95)00291-7

985 Clark, D., Lamare, M., Barker, M., 2009. Response of sea urchin pluteus larvae
986   (Echinodermata: Echinoidea) to reduced seawater pH: a comparison among a
987   tropical, temperate, and a polar species. Mar. Biol. 156, 1125–1137.
988   https://doi.org/10.1007/s00227-009-1155-8

989 Clarke, F.W., Wheeler, W.C., 1917. The inorganic constituents of marine
990   invertebrates. U.S. Geol. Surv. Prof. Pap. 102, 1–56.
991   https://doi.org/10.5962/bhl.title.11289

992 Cohen, A.L., Gaetani, G.A., Lundälv, T., Corliss, B.H., George, R.Y., 2006.
993   Compositional variability in a cold-water scleractinian, *Lophelia pertusa*: new
994   insights into "vital effects". Geochem. Geophys. Geosyst. 7, Q12004.
995   doi:10.1029/2006GC001354.

996 Crippa, G., Ye, F., Malinverno, C., Rizzi, A., 2016a. Which is the best method to
997   prepare invertebrate shells for SEM analysis? Testing different techniques on
998   recent and fossil brachiopods. Boll. Soc. Paleontol. Ital. 55, 111–125.
999   https://doi.org/10.4435/BSPI.2016.11

1000 Crippa, G., Angiolini, L., Bottini, C., Erba, E., Felletti, F., Frigerio, C., Hennissen,
1001   J.A.I., Leng, M.J., Petrizzo, M.R., Raffi, I., Raineri, G., Stephenson, M.H.,
1002   2016b. Seasonality fluctuations recorded in fossil bivalves during the early
1003   Pleistocene: Implications for climate change. Palaeogeography,
1004   Palaeoclimatology, Palaeoecology 446, 234–251.

1005 Curry, G.B., Brunton, C. H., 2007. Stratigraphic distribution of brachiopods, in:
1006   Selden, P.A. (Ed), Treatise on Invertebrate Paleontology. Part H, Brachiopoda.
1007   Geol. Soc. Am. & Univ. Kansas, New York, pp. 2901–3081.

1008   Cusack, M., Williams, A., 2007. Biochemistry & diversity of brachiopod shells. In:

1009   Kaesler, R. (Ed.), Treatise on Invertebrate Paleontology Part H, Brachiopoda.

1010   Geol. Soc. Am. & Univ. Kansas, New York, pp. 2373–2395.

1011   Cusack, M., Perez-Huerta, A., Janousch, M., Finch, A.A., 2008. Magnesium in the

1012   lattice of calcite shelled brachiopods. Chem. Geol. 257, 59–64.

1013   https://doi.org/10.1016/j.chemgeo.2008.08.007

1014   Cusack, M., Chung, P., Dauphin, Y., Perez-Huerta, A., 2010. Brachiopod primary

1015   layer crystallography and nanostructure. In: Alvarez, F., Curry, G.B. (Eds.),

1016   Evolution and Development of the Brachiopod Shell: Special Papers in

1017   Palaeontology Series, pp. 99–105.

1018   Cusack, M., Huerta A. P., EIMF, 2012. Brachiopods recording seawater

1019   temperature—A matter of class or maturation? Chem. Geol. 334, 139–143.

1020   https://doi.org/10.1016/j.chemgeo.2012.10.021

1021   Delaney, M. L., Popp, B. N., Lepzelter C. G., Anderson, T. F., 1989. Lithium-to-

1022   calcium ratios in modern, Cenozoic and Paleozoic articulate brachiopod shells.

1023   Paleoceanography 4, 681–691. https://doi.org/10.1029/PA004i006p00681

1024   Delaygue, G., Jouzel, J., Dutay, J. C., 2000. Oxygen 18–salinity relationship

1025   simulated by an oceanic general circulation model. Earth and Planetary Science

1026   Letters, 178(1-2), 113-123.

1027   Dellinger, M., West, A.J., Paris, G., Adkins, J.F., von Strandmann, P.A.P., Ullmann,

1028   C.V., Eagle, R.A., Freitas, P., Bagard, M.-L., Ries, J.B., Corsetti, F.A., Perez-

1029   Huerta, A., Kampf, A.R., 2018. The Li isotope composition of marine biogenic

1030   carbonates: Patterns and Mechanisms. Geochim Cosmochim Acta 236, 315-335.

DePaolo, D., 2011. Surface kinetic model for isotopic and trace element fractionation during precipitation of calcite from aqueous solutions. Geochim. Cosmochim. Acta 75, 1039–1056. https://doi.org/10.1016/j.gca.2010.11.020

Dickson, A. G., 1990. Thermodynamics of the dissociation of boric acid in synthetic seawater from 273.15 to 318.15 K. Deep-Sea Res. 37, 755–766. https://doi.org/10.1016/0198-0149(90)90004-F

Elderfield, H., Bertram, C. J., Erez, J., 1996. Biomineralization model for the incorporation of trace elements into foraminiferal calcium carbonate. Earth Planet. Sci. Lett. 142, 409–423. https://doi.org/10.1016/0012-821X(96)00105-7

England, J., Cusack, M., Lee, M.R., 2006. Magnesium and sulphur in the calcite shells of two brachiopods, *Terebratulina retusa* and *Novocrania anomala*. Lethaia 40, 2–10. https://doi.org/10.1111/j.1502-3931.2006.00001.x

Epstein, S., Buchsbaum, R., Lowenstam, H.A., Urey, H.C., 1953. Revised carbonate-water isotopic temperature scale. Bull. Geol. Soc. Am. 64, 1315–1326. https://doi.org/10.1130/0016-7606(1953)64[1315:RCITS]2.0.CO;2

Erez, J., 2003. The source of ions for biomineralization in foraminifera and their implications for paleoceanographic proxies. In: Dove, P. M., De Yoreo, J. J. & Weiner, S. (Ed.), Biomineralization. Rev. Mineral. Geochem., Washington, pp. 115–144. https://doi.org/10.2113/0540115

Evans, D., Erez, J., Oron, S., Müller, W., 2015. Mg/Ca-temperature and seawater-test chemistry relationships in the shallow dwelling large benthic foraminifera *Operculina ammonoides*. Geochim. Cosmochim. Acta 148, 325–342. https://doi.org/10.1016/j.gca.2014.09.039

1055   Foster, G., von Strandmann, P. A. E. P., Rae, J., 2010. Boron and magnesium isotopic

1056   composition of seawater. Geochem. Geophys. Geosyst. 11 (8), Q08015.

1057   https://doi.org/10.1029/2010GC003201

1058   Gabitov, R. I., Watson, E. B., 2006. Partitioning of strontium between calcite and

1059   fluid.   Geochem.   Geophys.   Geosyst.   7,   Q11004.

1060   https://doi.org/10.1029/2005GC001216

1061   Gabitov, R. I., Schmitt A., Rosner M., McKeegan D., Gaetani G., Cohen A., Watson

1062   E., Harrison, T., 2011. In situ δ^7Li, Li/Ca, and Mg/Ca analyses of synthetic

1063   aragonites.   Geochem.   Geophys.   Geosyst.   12:   Q03001.

1064   http://dx.doi.org/10.1029/ 2010GC003322.

1065   Gabitov, R. I., Sadekov, A., Leinweber, A., 2014. Crystal growth rate effect on

1066   Mg/Ca and Sr/Ca partitioning between calcite and fluid: An in situ approach.

1067   Chem. Geol. 367, 70–82. https://doi.org/10.1016/j.chemgeo.2013.12.019

1068   Gagnon, A.C., Adkins, J.F., Fernandez, D.P., Robinson, L.F., 2007. Sr/Ca and Mg/Ca

1069   vital effects correlated with skeletal architecture in a scleractinian deep-sea

1070   coral and the role of Rayleigh fractionation. Earth Planet. Sci. Lett. 261, 280–

1071   295. https://doi.org/10.1016/j.epsl.2007.07.013

1072   Garbelli, C., Angiolini, L., Brand, U., Shu-zhong, S., Jadoul, F., Posenato, R., Azmy,

1073   K., Chang-qun, C., 2016. Neotethys seawater chemistry and temperature at the

1074   dawn of the end Permian mass extinction. Gondwana Res., 35, 272-285.

1075   https://doi.org/10.1016/j.gr.2015.05.012

1076   Gaspard, D., Nouet, J., 2016. Hierarchical architecture of the inner layers of selected

1077   extant   rhynchonelliform   brachiopods.   J.   Struc.   Min.   196,   197–205.

1078   https://doi.org/10.1016/j.jsb.2016.07.021

1079   Gillikin, D.P., De Ridder, F., Ulens, H., Elskens, M., Keppens, E., Baeyens, W.,

1080   Dehairs, F., 2005. Assessing the reproducibility and reliability of estuarine

1081   bivalve shells (*Saxidomus giganteus*) for sea surface temperature reconstruction:

1082   implications for paleoclimate studies. Palaeogeography, Palaeoclimatology,

1083   Palaeoecology, 228(1-2), 70-85.

1084   Giuffre, A.J., Gagnon, A.C., De Yoreo, J.J., Dove, P.M., 2015. Isotopic tracer

1085   evidence for the amorphous calcium carbonate to calcite transformation by

1086   dissolution–reprecipitation. Geochim Cosmochim Acta 165, 407-417.

1087   Goetz, A.J., Griesshaber, E., Neuser, R.D., Lüter, C., Hühner, M., Harper, E.,

1088   Schmahl, W.W., 2009. Calcite morphology, texture and hardness in the distinct

1089   layers of rhynchonelliform brachiopod shells. Eur. J. Mineral. 21, 303–315.

1090   https://doi.org/10.1127/0935-1221/2009/0021-1922

1091   Goetz, A.J., Steinmetz, D.R., Griesshaber, E., Zaefferer, S., Raabe, D., Kelm, K.,

1092   Irsen, S., Sehrbrock, A., Schmahl, W.W., 2011. Interdigitating biocalcite

1093   dendrites form a 3-D jigsaw structure in brachiopod shells. Acta Biomater. 7,

1094   2237–2243. https://doi.org/10.1016/j.actbio.2011.01.035

1095   Gordon, C.M., Carr, R.A., Larson, R.E., 1970. The influence of environmental

1096   factors on the sodium and manganese content of barnacle shells. Limnol. Ocean.

1097   15, 461–466. https://doi.org/10.4319/lo.1970.15.3.0461

1098   Griesshaber, E., Schmahl, W.W., Neuser, R.D., Job, R., Bluem, M., Brand, U., 2005.

1099   Microstructure of brachiopod shells – an inorganic/organic fibre composite with

1100   nanocrystalline protective layer. In Katti, K., Ulm, G.J., Hellmich, C., & Viney,

1101   C. (eds.), Mechanical Properties of Bio-Inspired and Biological Materials, MRS

1102   Symp. Proc. Ser., 844, 99–104.

1103   Griesshaber, E., Kelm, K., Sehrbrock, A., Mader, W., Mutterlose, J., Brand, U.,

1104   Schmahl, W.W., 2009. Amorphous calcium carbonate in the shell material of

1105   the brachiopod *Megerlia truncata*. Eur. J. Mineral. 21, 715–723.

1106   https://doi.org/10.1127/0935-1221/2009/0021-1950

1107   Grossman, E.L., Mii, H.S., Yancey, T.E., 1993. Stable isotopes in Late Pennsylvanian

1108   brachiopods from the United States: implications for Carboniferous

1109   paleoceanography. Geol. Soc. Am. Bull. 105, 1284–1296.

1110   https://doi.org/10.1130/0016-7606(1993)105<1284:SIILPB>2.3.CO;2

1111   Grossman, E.L., Mii, H.S., Zhang, C., Yancey, T.E., 1996. Chemical variation in

1112   Pennsylvanian brachiopod shells; diagenetic, taxonomic, microstructural, and

1113   seasonal effects. J. Sediment. Res. 66 (5), 1011–1022.

1114   https://doi.org/10.1306/D4268469-2B26-11D7-8648000102C1865D

1115   Hartley, G., Mucci, A., 1996. The influence of pCO_2 on the partitioning of

1116   magnesium in calcite overgrowths precipitated from artificial seawater at 25 °C

1117   and 1 atm total pressure. Geochim. Cosmochim. Acta 60, 315–324.

1118   https://doi.org/10.1016/0016-7037(95)00388-6

1119   Hasse, B., Ehrenberg, H., Marxen, J.C., Becker, W., Epple, M., 2000, Calcium

1120   carbonate modifications in the mineralized shell of the freshwater snail

1121   *Biomphalaria glabrata*. Chem. Eur. J. 6 (20), 3679–3685.

1122   https://doi.org/10.1002/1521-3765(20001016)6:20<3679::AID-

1123   CHEM3679>3.0.CO;2-#

1124   Hemming, N. G., Hanson, G. N., 1992. Boron isotopic composition and

1125   concentration in modern marine carbonates. Geochim. Cosmochim. Acta 56,

1126   537–543. https://doi.org/10.1016/0016-7037(92)90151-8

1127   Immenhauser, A., Schöne, B., Hoffmann, R., Niedermayr, A., 2016. Mollusc and

1128   brachiopod skeletal hard parts: Intricate archives of their marine environment.

1129   Sedimentology 63, 1–59. https://doi.org/10.1111/sed.12231

1130   Ishikawa, M., Ichikuni, M., 1984. Uptake of sodium and potassium by calcite. Chem.

1131   Geol. 42, 137–146. https://doi.org/10.1016/0009-2541(84)90010-X

1132   Jacob, D. E., Soldati, A.L., Wirth, R., Huth, J., Wehrmeister, U., Hofmeister, W.,

1133   2008. Nanostructure, composition and mechanisms of bivalve shell growth.

1134   Geochim.   Cosmochim.   Acta   72   (22),   5401–5415.

1135   https://doi.org/10.1016/j.gca.2008.08.019

1136   Julliet-Leclerc, A., Rollion-Bard, C., Reynaud, S., Ferrier-Pagès, C., 2018. A new

1137   paradigm for $\delta^{18}O$ in coral skeleton oxygen isotope fractionation response to

1138   biological   kinetic   effects.   Chem.   Geol.   483,   131–140.

1139   https://doi.org/10.1016/j.chemgeo.2018.02.035

1140   Jurikova, H., Liebetrau, V., Gutjahr, M., Rollion-Bard, C., Hu, M.Y., Krause, S.,

1141   Henkel, D., Hiebenthal, C., Schmidt, M., Laudien, J., Eisenhauer, A., 2019.

1142   Boron isotope systematics of cultured brachiopod calcite: response to

1143   acidification, vital effects and implications for palaeo-pH reconstruction.

1144   Geochim. Cosmochim. Acta 248 ,370-386.

1145   Kim, S. T., O'Neil, J. R., 1997. Equilibrium and nonequilibrium oxygen isotope

1146   effects in synthetic carbonates. Geochim Cosmochim Acta 61 (16), 3461–3475.

1147   https://doi.org/10.1016/S0016-7037(97)00169-5

1148   Kitano, Y., Okumura, M., Idogaki M., 1975. Incorporation of sodium, chloride and

1149   sulfate   with   calcium   carbonate.   Geochem.   J.   9,   75–84.

1150   https://doi.org/10.2343/geochemj.9.75

1151   Kolodny, Y., Bar-Matthews, M., Ayalon, A., McKeegan, K. D., 2003. A high spatial
1152   resolution $\delta^{18}O$ profile of a speleotherm using an ion-microprobe. Chem.
1153   Geol. 197(1), 21–28. https://doi.org/10.1016/S0009-2541(02)00353-4

1154   Korte, C., Jones, P.J., Brand, U., Mertmann, D., Veizer, J., 2008. Oxygen isotope
1155   values from high-latitudes: clues for Permian sea-surface temperature gradients
1156   and Late Palaeozoic deglaciation. Palaeogeogr. Palaeoclimatol. Palaeoecol. 269,
1157   1–16. https://doi.org/10.1016/j.palaeo.2008.06.012

1158   Laudien, J., Jantzen, C., Häussermann, V., Försterra, G., 2014. Water temperature at
1159   time series station Liliguapi, Paso Comau, Patagonia, Chile in 2013/2014.
1160   Pangaea.

1161   Lea, D. W., Mashiotta, T. A., Spero, H. J., 1999. Controls on magnesium and
1162   strontium uptake in planktonic foraminifera determined by live culturing.
1163   Geochim. Cosmochim. Acta 63, 2369–2379. https://doi.org/10.1016/S0016-
1164   7037(99)00197-0

1165   Lea, D. W., Pak, D. K., Spero, H. J., 2000. Climate impact of Late Quaternary
1166   equatorial Pacific sea surface temperature variations. Science 289, 1719–1724.
1167   https://doi.org/10.1126/science.289.5485.1719

1168   Lee, X.Q., Hu, R.Z., Brand, U., Zhou, H., Liu, X.M., Yuan, H.L., Yan, C.L., Cheng,
1169   H.G., 2004. Ontogenetic trace element distribution in brachiopod shells: an
1170   indicator of original seawater chemistry. Chem. Geol. 209, 49–65.
1171   https://doi.org/10.1016/j.chemgeo.2004.04.029

1172   Lippmann, F., 1973. Sedimentary carbonate minerals. In: Von Engelhardt W., Hahn
1173   T., Roy R. & Wyllie P. J. (eds.), Mineral, Rocks and Inorganic Materials.
1174   Springer-Verlag. Berlin-Heidelberg, New York, pp 43–96.

1175 Littlewood, J., Shaw, S., Peacock, C.L., Bots, P., Trivedi, D., Burke, I.T., 2017.

1176   Mechanism of enhanced strontium uptake into calcite via an amorphous calcium

1177   carbonate (ACC) crystallisation pathway. Cryst. Growth Des. 17 (3), 1214-

1178   1223. https://doi.org/10.1021/acs.cgd.6b01599

1179 Lorens, R. B., 1981. Sr, Cd, Mn, and Co distribution coefficients in calcite as a

1180   function of calcite precipitation rate. Geochim. Cosmochim. Acta 45, 553–561.

1181 Lorens, R.B., Bender, M.L., 1977. Physiological exclusion of magnesium from

1182   *Mytilus edulis* calcite. Nature 269, 793–794. https://doi.org/10.1016/0016-

1183   7037(81)90188-5

1184 Lowenstam, H., 1961. Mineralogy, O^{18}/O^{16} ratios and strontium and magnesium

1185   content of recent and fossil brachiopods and their bearing on the history of the

1186   oceans. J. Geol. 69 (3), 241–260.

1187 Lowenstam, H. A., Weiner, S., 1989. On Biomineralization. Oxford University Press,

1188   New York, 324 pp.

1189 MacKinnon, D.I., Williams, A., 1974. The shell structure in spiriferide brachiopoda.

1190   Bull. Br. Mus. Geol. 5 (3), 189–258.

1191 Marriott, C. S., Henderson, G. M., Belshaw, N. S., Tudhope, A.W., 2004.

1192   Temperature dependence of δ^7Li, $\delta^{44}Ca$ and Li/Ca during growth of calcium

1193   carbonate.   Earth   Planet.   Sci.   Lett.   222,   615–624.

1194   https://doi.org/10.1016/j.epsl.2004.02.031

1195 Mass, T., Giuffre, A.J., Sun, C-H., Stifler, C.A., Frazier, M.J., Neder, M., Tamura, N.,

1196   Stan, C.V., Marcus, M.A., Gilbert, P., 2017. Amorphous calcium carbonate

1197   particles form coral skeletons. Proc. Natl. Acad. Sci. USA 114 (37), 7670–7678.

1198   https://doi.org/10.1073/pnas.1707890114

1199   Mavromatis, V., Gautier, Q., Bosc, O., Schott, J., 2013. Kinetics of Mg partition and

1200   Mg stable isotope fractionation during its incorporation in calcite. Geochim.

1201   Cosmochim. Acta 114, 188–203. https://doi.org/10.1016/j.gca.2013.03.024

1202   Mavromatis, V., Purgstaller, B., Dietzel, M., Buhl, D., Immenhauser, A., Schott, J.,

1203   2017. Impact of amorphous precursor phases on magnesium isotope signatures

1204   of Mg-calcite. Earth Planet. Sci. Lett. 464, 227–236.

1205   https://doi.org/10.1016/j.epsl.2017.01.031

1206   McConnaughey, T., 1989a. ^{13}C and ^{18}O isotopic disequilibrium in biological

1207   carbonates: I. Patterns. Geochim. Cosmochim. Acta 53(1), 151–162.

1208   https://doi.org/10.1016/0016-7037(89)90282-2

1209   McConnaughey, T., 1989b. ^{13}C and ^{18}O isotopic disequilibrium in biological

1210   carbonates: II. In vitro simulation of kinetic isotope effects. Geochim.

1211   Cosmochim. Acta 53(1), 163–171. https://doi.org/10.1016/0016-

1212   7037(89)90283-4

1213   McConnaughey, T. A., Burdett, J., Whelan, J. F., Paul, C. K., 1997. Carbon isotopes

1214   in biological carbonates: respiration and photosynthesis. Geochim. Cosmochim.

1215   Acta 61(3), 611–622. https://doi.org/10.1016/S0016-7037(96)00361-4

1216   McCrea, J.M., 1950. On the isotopic chemistry of carbonates and a paleotemperature

1217   scale. J. Chem. Phys. 18, 849–857. https://doi.org/10.1063/1.1747785

1218   Meibom, A., Cuif, J.P., Hillion, F.O., Constantz, B.R., Juillet-Leclerc, A., Dauphin,

1219   Y., Watanabe, T., Dunbar, R.B., 2004. Distribution of magnesium in coral

1220   skeleton. Geophys. Res. Lett. 31, L23306.

1221   https://doi.org/10.1029/2004GL021313

1222 Millero, F.J., 1995. Thermodynamics of the carbon dioxide system in the oceans.

1223 Geochim. Cosmochim. Acta 59, 661–677. https://doi.org/10.1016/0016-

1224 7037(94)00354-O

1225 Morse, J. W., Bender, M. L., 1990. Partition coefficients in calcite: Examination of

1226 factors influencing the validity of experimental results and their application to

1227 natural systems. Chem. Geol. 82, 265–277. https://doi.org/10.1016/0009-

1228 2541(90)90085-L

1229 Mucci, A., Morse, J. W., 1983, The incorporation of Mg^{2+} and Sr^{2+} into calcite

1230 overgrowths: Influences of growth rate and solution composition. Geochim.

1231 Cosmochim. Acta 47, 217–233. https://doi.org/10.1016/0016-7037(83)90135-7

1232 Nielsen, L.C., DePaolo, D.J., De Yoreo, J.J., 2012. Self-consistent ion-by-ion growth

1233 model for kinetic isotopic fractionation during calcite precipitation. Geochim.

1234 Cosmochim. Acta 86, 166–181. https://doi.org/10.1016/j.gca.2012.02.009

1235 Nûrnberg, D., Bijma, J., Hemleben, C., 1996. Assessing thereliability of magnesium

1236 in foraminiferal calcite as a proxy for water mass temperature. Geochim.

1237 Cosmochim. Acta 60, 803– 814. https://doi.org/10.1016/0016-7037(95)00446-7

1238 O'Neil, J.R., Clayton, R.N., Mayeda, T.K., 1969. Oxygen isotope fractionation in

1239 divalent metal carbonates. J. Chem. Phys. 51, 5547–5558.

1240 https://doi.org/10.1063/1.1671982

1241 Okumura, M., Kitano, Y., 1986. Coprecipitation of alkali metal ions with calcium

1242 carbonate. Geochim. Cosmochim. Acta 50, 49–58.

1243 https://doi.org/10.1016/0016-7037(86)90047-5

1244 Oomori, T., Kaneshima, H, Maezato, Y., 1987. Distribution coefficient of Mg^{2+} ions

1245 between calcite and solution at 10-50°C. Mar. Chem. 20, 327–336.

1246 https://doi.org/10.1016/0304-4203(87)90066-1

1247   Paine, R.T., 1969. Growth and size distribution of the brachiopod *Terebratalia*

1248   *transversa* (Sowerby). Pac. Sci. 23, 337–343.

1249   Parkinson, D., Curry, G. B., Cusack, M., Fallick, A. E., 2005. Shell structure, patterns

1250   and trends of oxygen and carbon stable isotopes in modern brachiopod shells.

1251   Chem. Geol. 219, 193–235. https://doi.org/10.1016/j.chemgeo.2005.02.002

1252   Peck, L.S., Brockington, S., Brey, T., 1987. Growth and metabolism in the Antarctic

1253   brachiopod *Liothyrella uva*. Philos. Trans. R. Soc. Lond. B Biol. Sci. 352, 851–

1254   858. https://doi.org/10.1098/rstb.1997.0065

1255   Penman, D. E., Hönisch, B., Rasbury, E. T., Hemming, N. G., Spero, H.J., 2013.

1256   Boron, carbon, and oxygen isotopic composition of brachiopod shells: intra-

1257   shell variability, controls, and potential as a paleo-pH recorder. Chem. Geol.

1258   340, 32–39. https://doi.org/10.1016/j.chemgeo.2012.11.016

1259   Perez-Huerta, A., Cusack, M., Jeffries, T.E., Williams, C.T., 2008. High resolution

1260   distribution of magnesium and strontium and the evaluation of Mg/Ca

1261   thermometry in Recent brachiopod shells. Chem. Geol. 247, 229–241.

1262   https://doi.org/10.1016/j.chemgeo.2007.10.014

1263   Perez-Huerta, A., Cusack, M., McDonald, S., Marone, F., Stampanoni, M., MacKay,

1264   S., 2009. Brachiopod punctae: A complexity in shell biomineralization. J.

1265   Struct. Bio. 167, 62-69. https://doi.org/10.016/j.jsb.2009.03.013

1266   Politi, Y., Batchelor, D.R., Zaslansky, P., Chmelka, B.F., Weaver, J.C., Sagi, I.,

1267   Weiner, S., Addadi, L., 2009. Role of magnesium ion in the stabilization of

1268   biogenic amorphous calcium carbonate: a structure–function investigation.

1269   Chem. Mater. 22, 161–166. https://doi.org/10.1021/cm902674h

1270   Popp, B.N., Anderson, T.F., Sandberg, P.A., 1986. Textural, elemental and isotopic

1271   variations among constituents in Middle Devonian limestones, North America.

1272   J. Sediment. Petrol. 56, 715–727. https://doi.org/10.1306/212F8A26-2B24-

1273   11D7-8648000102C1865D

1274   Powell, M.G., Schöne, B.R. Jacob, D.E., 2009. Tropical marine climate during the

1275   late Paleozoic ice age using trace element analyses of brachiopods. Palaeogeogr.

1276   Palaeoclimatol. Palaeoecol. 280(1-2),143-149.

1277   https://doi.org/10.1016/j.palaeo.2009.06.003

1278   Raz, S., Testeniere, O., Hecker, A., Weiner, S., Luquet, G., 2002. Stable Amorphous

1279   Calcium Carbonate Is the Main Component of the Calcium Storage Structures

1280   of the Crustacean *Orchestia cavimana.* Biol. Bull. 203, 269–274.

1281   https://doi.org/10.2307/1543569

1282   Robinson, L., Adkins, J.F., Gagnon, A., Prouty, N., Roark, B., van der Flierdt, T.,

1283   2014. The geochemistry of deep-sea coral skeletons: applications for

1284   paleoceanography. Deep- Sea Res. II 99, 184–198.

1285   https://doi.org/10.1016/j.dsr2.2013.06.005

1286   Rollion-Bard, C., Marin-Carbonne, J., 2011. Measurements of SIMS matrix effects on

1287   oxygen isotopic compositions in carbonates. J. Anal. Atom. Spectrom. 26,

1288   1285–1289. https://doi.org/10.1039/C0JA00213E

1289   Rollion-Bard, C., Blamart, D., 2014. SIMS method and examples of applications in

1290   coral biomineralization. In: DiMasi, E., Gower, L.B., (Eds.), Biomineralization

1291   Sourcebook: Characterization of Biominerals and Biomimetic Materials. CRC

1292   Press: Boca Raton, FL, USA, pp. 249–261

1293   Rollion-Bard, C., Blamart, D., 2015. Possible controls on Li, Na, and Mg

1294   incorporation into aragonite coral skeletons. Chem. Geol. 396, 98–111.

1295   https://doi.org/10.1016/j.chemgeo.2014.12.011

1296   Rollion-Bard, C., Chaussidon, M., France-Lanord, C., 2003. pH control on oxygen

1297   isotopic composition of symbiotic corals. Earth Planet. Sci. Lett. 215, 275–288.

1298   https://doi.org/10.1016/S0012-821X(03)00391-1

1299   Rollion-Bard, C., Mangin, D., Champenois, M., 2007. Development and application

1300   of oxygen and carbon isotopic measurements of biogenic carbonates by ion

1301   microprobe. Geostand. Geoanal. Res. 31, 39–50. https://doi.org/10.1111/j.1751-

1302   908X.2007.00834.x

1303   Rollion-Bard, C., Erez, J., Zilberman, T., 2008. Intra-shell oxygen isotope ratios in the

1304   benthic genus Amphistegina and the influence of seawater carbonate chemistry

1305   and temperature on this ratio. Geochim. Cosmochim. Acta 72, 6006–6014.

1306   https://doi.org/10.1016/j.gca.2008.09.013

1307   Rollion-Bard, C., Blamart, D., Cuif, J.-P., Dauphin, Y., 2010. In situ measurements of

1308   oxygenisotopic composition in deep-sea coral, *Lophelia pertusa*: re-examination

1309   of the current geochemical models of biomineralization. Geochim. Cosmochim.

1310   Acta 74, 1338–1349. https://doi.org/10.1016/j.gca.2009.11.011

1311   Rollion-Bard, C., Chaussidon, M., France-Lanord, C., 2011. Biological control of

1312   internal pH in scleractinian corals: Implications on paleo-pH and paleo-

1313   temperature reconstructions. C. R. Geosci. 343(6), 397–405.

1314   https://doi.org/10.1016/j.crte.2011.05.003

1315   Rollion-Bard, C., Saulnier, S., Vigier, N., Schumacher, A., Chaussidon, M., Lécuyer,

1316   C., 2016. Variability in magnesium, carbon and oxygen isotope compositions of

1317   brachiopod shells: Implications for paleoceanographic studies. Chem. Geol.

1318   423, 49–60. https://doi.org/10.1016/j.chemgeo.2016.01.007

1319   Romanin, M., Crippa, G., Ye, F., Brand, U., Bitner, M.A., Gaspard, D., Häussermann,

1320   V., Laudien, J. A., 2018. Sampling strategy for recent and fossil brachiopods:

1321   selecting the optimal shell segment for geochemical analyses. Riv. Ital.

1322   Paleontol. S. 124(2), 343-359. https://doi.org/10.13130/2039-4942/10193

1323 Rosenthal, Y., Morley, A., Barras, C., Katz, M. E., Jorissen, F., Reichart, G. J., Oppo,

1324   D. W., Linsley, K. L., 2011. Temperature calibration of Mg/Ca ratios in the

1325   intermediate water benthic foraminifer *Hyalinea balthica*. Geochem. Geophys.

1326   Geosyst. 12, Q04003. https://doi.org/10.1029/2010GC003333

1327 Rucker, J.B., Valentine, J.W., 1961. Salinity response of trace element concentration

1328   in *Crassostrea virginica.* Nature 190, 1099–1100.

1329   https://doi.org/10.1038/1901099a0

1330 Schöne, B.R., Surge, D.M., 2012. Part N, Revised, Volume 1, Chapter 14: Bivalve

1331   sclerochronology and geochemistry. Treat. Online 46, pp. 1–24.

1332 Schöne, B. R., Zhang, Z., Jacob, D., Gillikin, D.P., Tütken, T., Garbe-Schönberg, D.,

1333   McConnaughey, T., Soldati, A., 2010. Effect of organic matrices on the

1334   determination of the trace element chemistry (Mg, Sr, Mg/Ca, Sr/Ca) of

1335   aragonite bivalve shells (*Arctica islandica*) – comparison of ICP-OES and LA-

1336   ICP-MS data. Geochem J. 44, 23– 37. https://doi.org/10.2343/geochemj.1.0045

1337 Steuber, T., Veizer, J., 2002. Phanerozoic record of plate tectonic control of seawater

1338   chemistry and carbonate sedimentation. Geology 30, 1123–1126.

1339   https://doi.org/10.1130/0091-7613(2002)030<1123:PROPTC>2.0.CO;2

1340 Sylvester, P. J., 2008. Matrix effects in laser ablation ICP-MS. In: Laser ablation ICP-

1341   MS in the earth sciences: Current practices and outstanding issues.

1342   Mineralogical Association of Canada. p. 67-78.

1343 Takayanagi, H., Asami, R., Abe, O., Miyajima, T., Kitagawa, H., Iryu, Y., 2012.

1344   Carbon- and oxygen-isotope compositions of a deep-water modern brachiopod

1345   *Campagea japonica* collected off Aguni-jima, Central Ryukyu Islands,

1346   southwestern   Japan.   Geochem.   J.   46,   77–87.

1347   https://doi.org/10.2343/geochemj.1.0153

1348 Takayanagi, H., Asami, R., Abe, O., Miyajima, T., Kitagawa, H., Sasaki, K., Iryu, Y.,

1349   2013. Intraspecific variations in carbon- and oxygen-isotope compositions of a

1350   brachiopod *Basiliola lucida* collected off Okinawa-jima, southwestern Japan.

1351   Geochim.   Cosmochim.   Acta   115,   115–136.

1352   https://doi.org/10.1016/j.gca.2013.03.026

1353 Tang J., Köhler S. J., Dietzel M., 2008. Sr^{2+}/Ca^{2+} and $^{44}Ca/^{40}Ca$ fractionation during

1354   inorganic calcite formation: I. Sr incorporation. Geochim. Cosmochim. Acta 72,

1355   3718–3732. https://doi.org/10.1016/j.gca.2008.05.031

1356 Thompson, R.E., 1981. Oceanography of the British Columbia coast. Can. Spec. Publ.

1357   Fish. Aquat. Sci., 50, 1-291.

1358 Ullmann, C.V., Campbell, H.C., Frei, R., Korte, C., 2016. Oxygen and carbon isotope

1359   and Sr/Ca signatures of high-latitude Permian to Jurassic calcite fossils from

1360   New   Zealand   and   New   Caledonia.   Gondwana   Res.   38,   60   –   73.

1361   https://doi.org/10.1016/j.gr.2015.10.010

1362 Ullmann, C. V., Frei, R., Korte, C., Lüter, C., 2017. Element/Ca, C and O isotope

1363   ratios in modern brachiopods: Species-specific signals of biomineralization.

1364   Chem. Geol. 460, 15–24. https://doi.org/10.1016/j.chemgeo.2017.03.034

1365 Usdowski, E., Hoefs, J., 1993. Oxygen isotope exchange between carbonic acid,

1366   bicarbonate, carbonate, and water: a re-examination of the data of McCrea

1367   (1950) and an expression for the overall partitioning of oxygen isotopes

1368   between the carbonate species and water. Geochim. Cosmochim. Acta 57 (15),

1369   3815–3818. https://doi.org/10.1016/0016-7037(93)90159-T

1370   Usdowski, E., Michaelis, J., Böttcher, M.E., Hoefs, J., 1991. Factors for the oxygen

1371   isotope equilibrium fractionation between aqueous and gaseous CO_2, carbonic

1372   acid, bicarbonate, carbonate, and water (19 °C). Z. Phys. Chem 170, 237–249.

1373   https://doi.org/10.1016/0016-7037(93)90159-T

1374   Veizer, J., Ala, D., Azmy, K., Bruckschen, P., Buhl, D., Bruhn, F., Carden, G.A.F.,

1375   Diener, A., Ebneth, S., Godderis, Y., Jasper, T., Korte, C., Pawellek, F.,

1376   Podlaha, O.G., Strauss, H., 1999. $^{87}Sr/^{86}Sr$, $\delta^{13}C$ and $\delta^{18}O$ evolution of

1377   Phanerozoic seawater. Chem. Geol. 161, 59–88. https://doi.org/10.1016/S0009-

1378   2541(99)00081-9

1379   Vengosh, A., Kolodny, Y., Starinsky, A., Chivas, A.R., McCulloch, M.T., 1991.

1380   Coprecipitation and isotopic fractionation of boron in modern biogenic

1381   carbonates. Geochim. Cosmochim. Acta 55, 2901–2910.

1382   https://doi.org/10.1016/0016-7037(91)90455-E

1383   Vidavsky, N., Addadi, S., Schertel, A., Ben-Ezra, D., Shpigel, M., Addadi, L.,

1384   Weiner, S., 2016. Calcium transport into the cells of the sea urchin larva in

1385   relation to spicule formation. Proc. Natl. Acad. Sci. USA 113,12637–12642.

1386   https://doi.org/10.1073/pnas.1612017113

1387   Watkins, J.M., Nielsen, L.C., Ryerson, F.J., DePaolo, D.J., 2013. The influence of

1388   kinetics on the oxygen isotope composition of calcium carbonate. Earth Planet.

1389   Sci. Lett. 375, 349–360. https://doi.org/10.1016/j.epsl.2013.05.054

1390   Watson, E.B., 2004. A conceptual model for near-surface kinetic controls on the trace

1391   element and stable isotope composition of abiogenic calcite crystals. Geochim.

1392   Cosmochim. Acta 68 (7), 1473–1488. https://doi.org/10.1016/j.gca.2003.10.003

1393   Watson, E. B., Liang, Y., 1995. A simple model for sector zoning in slowly grown

1394   crystals: Implications for growth rate and lattice diffusion, with emphasis on

1395 accessory minerals in crustal rocks. Am. Mineral. 80, 1179–1187.

1396 https://doi.org/10.2138/am-1995-11-1209

1397 Weiner, S., Addadi, L., 2011. Crystallization pathways in biomineralization. Annual

1398 review of materials research 41, 21-40.

1399 Weiss, A., 2003. Mineralization in organic matrix frameworks. Rev. Mineral.

1400 Geochem. 54, 249–283. https://doi.org/10.2113/0540249

1401 Weiss, I.M., Tuross, N., Addadi, L., Weiner, S., 2002. Mollusk larval shell formation:

1402 amorphous calcium carbonate is a precursor for aragonite. J. Exp. Zool. 293,

1403 478–491. https://doi.org/10.1002/jez.90004

1404 Wenzel, B., Joachimski, M.M., 1996. Carbon and oxygen isotopic composition of

1405 Silurian brachiopods (Gotland/Sweden): palaeoceanographic implications.

1406 Palaeogeogr. Palaeoclimatol. Palaeoecol. 122, 143–166.

1407 https://doi.org/10.1016/0031-0182(95)00094-1

1408 Williams, A., 1966. Growth and structure of the shell of living articulate brachiopods.

1409 Nature 10, 1146–1148. https://doi.org/10.1038/2111146a0

1410 Williams, A., 1968. Evolution of the shell structure of articulate brachiopods. Spec.

1411 Pap. Paleontol. 2, 1–55.

1412 Williams, A., 1997. Shell structure. In: Kaesler, R.L. (Ed.), Treatise on Invertebrate

1413 Palaeontology (Part H, Brachiopoda Revised). Introduction. Geological Society

1414 of America, vol. 1. University of Kansas Press, Boulder, CO, pp. 267–320

1415 (Lawrence).

1416 Wit, J. C., de Nooijer, L. J., Wolthers, M., Reichart, G. J., 2013. A novel salinity

1417 proxy based on Na incorporation into foraminiferal calcite. Biogeosciences 10,

1418 6375–6387. https://doi.org/10.5194/bg-10-6375-2013

1419   Wolf, S.E., Leiterer, J., Kappl, M., Emmerling, F., Tremel, W., 2008. Early homogenous amorphous precursor stages of calcium carbonate and subsequent crystal growth in levitated droplets. Journal of the American Chemical Society 130, 12342-12347.

1423   Yamamoto, K., Asami, R., Iryu, Y., 2010. Within-shell variations in carbon and oxygen isotope compositions of two modern brachiopods from a subtropical shelf environment off Amami-o-shima, southwestern Japan. Geochem. Geophys. Geosyst. 11, Q10009. https://doi.org/10.1029/2010GC003190

1427   Yamamoto, K., Asami, R., Iryu, Y., 2011. Brachiopod taxa and shell portions reliably recording past ocean environments: Toward establishing a robust paleoceanographic proxy. Geophys. Res. Lett. 38, L13601. https://doi.org/10.1029/2011GL047134

1431   Yamamoto, K., Asami, R., Iryu, Y., 2013. Correlative relationships between carbon- and oxygen-isotope records in two cool-temperate brachiopod species off Otsuchi Bay, northeastern Japan. Paleontol. Res. 16, 12–26. https://doi.org/10.2517/1342-8144-17.1.12

1435   Ye, F., Crippa, G., Angiolini, L., Brand, U., Capitani, G.C., Cusack, M., Garbelli, C., Griesshaber, E., Harper, E., Schmahl, W., 2017. Mapping of recent brachiopod microstructure: A tool for environmental studies. J. Struct. Biol. 201, 221–236. https://doi.org/10.1016/j.jsb.2017.11.011

1439   Ye, F., Jurikova, H., Angiolini, L., Brand, U., Crippa, G., Henkel, D., Laudien, J., Hiebenthal, C., Šmajgl, D., 2019. Variation in brachiopod microstructure and isotope geochemistry under low-pH – ocean acidification conditions. Biogeosciences 16, 1–26.

1443   Zeebe, R. E., 1999. An explanation of the effect of seawater carbonate concentration
1444   on foraminiferal oxygen isotopes. Geochim. Cosmochim. Acta, 63, 2001-2007,
1445   https://doi.org/10.1016/S0016-7037(99)00091-5

1446   Zeebe, R. E., 2001. Seawater pH and isotopic paleotemperatures of Cretaceous
1447   oceans. Palaeogeogr. Palaeoclimatol. Palaeoecol. 170, 49–57.
1448   https://doi.org/10.1016/S0031-0182(01)00226-7

1449   Zeebe, R.E., 2007. An expression of the overall oxygen isotope fractionation between
1450   the sum of dissolved inorganic carbon and water. Geochem. Geophys. Geosyst.
1451   8, Q09002. https://doi.org/10.1029/2007GC001663

1452   Zeebe, R. E., Wolf-Gladrow, D.A., 2001. CO_2 in seawater: Equilibrium, kinetics,
1453   isotopes. Elsevier Oceanography Series, 65. Elsevier, 346 pp.

1454   Zeebe, R.E., Sanyal, A., 2002. Comparison of two potential strategies of planktonic
1455   foraminifera for house building: Mg^{2+} or H^+ removal? Geochim. Cosmochim.
1456   Acta 66 (7), 1159–1169. https://doi.org/10.1016/S0016-7037(01)00852-3

1457   Zhang, Y., Dave, R.A., 2000. Influence of Mg^{2+} on the kinetics of calcite precipitation
1458   and calcite crystal morphology. Geochim. Cosmochim. Acta 163, 129–138.
1459   https://doi.org/10.1016/S0009-2541(99)00097-2

1460   Zhang, Z., Robson, S.P., Emig, C., Shu, D., 2008. Early Cambrian radiation of
1461   brachiopods: a perspective from South China. Gondwana Res. 14, 241–254.
1462   https://doi.org/10.1016/j.gr.2007.08.001

1463   **Tables and Figures**

1464   Figure 1. Location of brachiopod sampling. (1) San Juan Islands, Washington, USA

1465   (48.5°N, 123°W): *Terebratalia transversa*. (2) Isla Jaime, Ensenada de las Islas, Chile

1466   (43.8°S, 72.9°W): *Magellania venosa*. (3) Tuscan Archipelago, Italy (42.3°N, 9.9°E):

1467   *Gryphus vitreus*. (4) Doubtful Sound, New Zealand (45.4°S, 167.1°E): *Magasella*

1468   *sanguinea, Calloria inconspicua, Liothyrella neozelanica, Notosaria nigricans*.

1469

1470   Figure 2. Illustrative scheme of the parts used for analyses carried out in a valve of a

1471   brachiopod specimen (*M. venosa,* MV05). The upper half of the valve shows how it

1472   was mounted in an aluminium ring and embedded into epoxy for in-situ analyses (i.e;

1473   ion microprobe and/or laser ablation); the lower half was prepared and crushed into

1474   powder for bulk $\delta^{18}O$ and $\delta^{13}C$ analyses.

1475

1476   Figure 3. Pictures of ion probe spots in the shell of *N. nigricans* (a) Photograph of the

1477   ventral valve of *N. nigricans* analysed for oxygen isotopes in the central and anterior

1478   parts (circled in red). (b) SEM picture of the ion probe spots in the dorsal valve of *N.*

1479   *nigricans*. The picture belongs to the profile 428d@200, measured in the anterior part.

1480   (Supplementary Table 2)

1481

1482   Figure 4. Secondary electron microscopy images of the brachiopod shell

1483   microstructures: (a) Terebratulid *M. venosa*, composed of primary and secondary

1484   layers; (b) Rhynchonellid *N. nigricans*, composed of primary and secondary layers,

1485   and (c) Terebratulid *L. neozelanica*, composed of primary, secondary and tertiary

1486   layers. PL: primary layer, SL: secondary layer, TL: tertiary layer, p: punctae.

1487

1488   Figure 5. Oxygen isotopic composition from the outermost to innermost shell in the

1489   central and anterior parts of modern brachiopod species (a) *T. transversa*, (b) *M.*

1490   *sanguinea*, (c) *M. venosa,* (d) *N. nigricans*, (e) *L. neozelanica*, and (f) *G. vitreus*.

1491   Error bars represent the standard deviation. Grey fields indicate the region of $\delta^{18}O$

1492   values for inorganic calcite precipitated in equilibrium with seawater for each locality

1493   according to the equation of Watkins et al. (2013). The relative distance is calculated

1494   with 0% corresponding to the outermost part of the shell and 100% the innermost

1495   part. Closed circles are for measurements in the ventral valve and open circles for

1496   measurements in the dorsal valve. Black lines are for measurements in the central part

1497   and dotted lines for measurements in the anterior part. Red circles represent

1498   measurements in the primary layer, black circles in the secondary layer and blue

1499   circles in the tertiary layer. The dotted horizontal lines represent the bulk $\delta^{18}O$ values.

1500   T: terebratulid brachiopod, R: rhynchonellid brachiopod.

1501

1502   Figure 6. Li/Ca, Na/Ca, Mg/Ca and Sr/Ca variations from outermost to innermost

1503   shell in the central and anterior parts of the modern brachiopod species *M. sanguinea*,

1504   *N. nigricans* and *G. vitreus*. The secondary y-axis represents the ratio between the

1505   partition coefficient calculated for brachiopod calcite relative to seawater and the

1506   partition coefficient of inorganic calcite in equilibrium ($E_{b-i.c}$, see text for more

1507   explanations). Grey line indicates the value of equilibrium (by definition, $E_{b-i.c}=1$).

1508   Error bars represent the standard deviation. Closed circles are for measurements in the

1509   ventral valve and open circles for measurements in the dorsal valve. Red circles

1510   represent measurements in the primary layer, black circles in the secondary layer and

1511   blue circles in the tertiary layer.

1512

1513   Figure 7. Measured $\delta^{18}O$ values in the modern brachiopod species and the calculated

1514   expected equilibrium $\delta^{18}O$ values according to various paleotemperature equations.

1515   (a) *T. transversa*, (b) *M. sanguinea*, (c) *M. venosa*, (d) *N. nigricans*, (e) *L. neozelanica*

1516   and (f) *G. vitreus.* 1: Brand et al. (2013), 2: Kim and O'Neil. (1997), 3: Anderson and

1517   Arthur (1983), 4: O'Neil et al. (1969), 5: Epstein et al. (1953), 6: Watkins et al.

1518   (2013). PL: Primary layer. SL: Secondary layer. TL: Tertiary layer. Solid lines

1519   represent $\delta^{18}O$ –T calibrations for inorganic calcite. Hatched line represents $\delta^{18}O$ –T

1520   calibrations for biogenic calcite.

1521

1522   Figure 8. (a) Sr/Ca vs $\delta^{18}O$ values and (b) Na/Ca vs Sr/Ca in the secondary layer of

1523   modern brachiopod species. Error bars represent the standard deviation.

1524

1525   Figure 9. Li/Ca, Na/Ca, Mg/Ca and Sr/Ca partition coefficients (D_{Li}, D_{Na}, D_{Mg} and

1526 D_{Sr}) of the average values, i.e. plateau zone, measured in the innermost secondary

1527   layer brachiopod calcite and D_{Li} and D_{Sr} of inorganic calcite (black triangles and

1528   squares) versus environmental parameters (temperature, pH and salinity). Data of the

1529   literature are from Delaney et al (1989), Butler et al (2015) (grey triangles), Dellinger

1530   et al (2018), Brand et al (2013) (crosses) and Perez-Huerta et al (2008). Values for

1531   inorganic calcite are from Marriott et al (2004) for lithium and DePaolo (2011) for

1532   strontium. Error bars represent the standard deviation.

1533

1534 Table 1. List of species, site of collection and temperature, salinity and pH (seawater

1535 scale) of the ambient seawater. PL: Primary layer, SL: secondary layer, TL: tertiary

1536 layer, V: ventral, D: dorsal. Seawater temperatures, salinities and pH are taken from:

1537 [1]Thomson (1981), [2]Penman et al. (2013), [3]Brand et al. (2013), [4]Laudien et al. (2014),

1538 [5]Bajnai et al. (2018), [6]Ye et al (2018); [7]MEDATLAS, [8]this study, [9]Clark et al. (2009),.

1539 T: Terebratulida, R: Rhynchonellida

Species	Order	Shell layer	Number of specimens	Locality	Water depth (m)	T (°C)	Salinity	pH	$\delta^{18}O_{sw}$ (‰ SMOW)
Terebratalia transversa	T	PL, SL	3	San Juan Islands	64	7.3-11.1[1]	29.7-30.5[1]	7.71[2]	-1.8[3]
Magellania venosa	T	PL, SL	2	Isla Jaime	22	9.3-12.7[4]	32.5-33[4]	7.95[4]	-1.2[5]
Gryphus vitreus	T	PL, SL, TL	3	Tuscan Archipelago	140-160	13.2-16.8[3]	39[6]	8.2[7]	1.2[3]
Magasella sanguinea	T	PL, SL	4						
Calloria inconspicua	T	PL, SL	1	Doubtful Sound	20	7-17.6[8]	32.1-35.4[8]	7.96[9]	0.3[3]
Notosaria nigricans	R	PL, SL	3						
Liothyrella neozelanica	T	PL, SL, TL	1						

1540
1541

1542

1543   Table 2. Ventral and dorsal valve lengths and valve width of the brachiopod

1544   specimens studied here. -: not measured.

Species	Sample ID	Ventral valve length (mm)	Dorsal valve length (mm)	Valve width (mm)
T. transversa	D500L	27.1	-	30.0
	D501L	26.2	22.6	29.1
	D504L	23.1	19.7	28.1
M. sanguinea	DS401L	31.05	27.25	32.9
	DS402L	24.8	21.1	25.2
	DS403L	31.1	26.4	33.0
	DS404L	34.55	29.7	32.2
N. nigricans	DS428L	18.25	15.9	15.9
	DS429L	-	-	-
	DS430L	-	-	-
G. vitreus	GV13	33	30	28.5
	GV47	34	30	29
	GV78	36	31	30
M. venosa	MV05	48	42.5	39
	MV17	25	21.5	22.5
L. neozelanica	DS422L	33	29.6	31
C. inconspicua	DS419L	19.9	16.9	17.9

1545

1546

1547   Table 3. $\delta^{18}O$ (‰, V-PDB) and $\delta^{13}C$ (‰, V-PDB) of the secondary layer (± tertiary

1548   layer) measured by bulk technique. -: not measured

Species	Sample ID	$\delta^{18}O$	SD	$\delta^{13}C$	SD
T. transversa	D500L	-0.70	0.07	-0.80	0.16
	D501L	-1.09	0.02	-1.79	0.04
	D504L	-0.65	0.07	-0.68	0.15
M. sanguinea	DS401L	0.42	0.04	0.58	0.08
	DS402L	0.14	0.05	0.27	0.08
	DS403L	-0.07	0.04	0.02	0.07
	DS404L	-0.22	0.04	-0.14	0.08
N. nigricans	DS428L	1.08	0.14	1.33	0.08
	DS429L	0.52	0.17	1.27	0.10
	DS430L	1.02	0.11	0.42	0.03
G. vitreus	GV13	2.28	0.21	2.85	0.05
	GV47	2.08	0.10	2.71	0.03
	GV78	1.99	0.15	2.82	0.06
M. venosa	MV05	-	-	-	-
	MV17	-0.78	0.02	-1.07	0.05
L. neozelanica	DS422L	0.59	0.06	1.36	0.08
C. inconspicua	DS419L	0.34	0.03	0.43	0.06

1549
1550

1551

1552 Table 4. Significant (p<0.05) linear regression and statistics of the relations between

1553 different elemental ratios in the brachiopod calcite and their environmental

1554 parameters. The standard error for the slope and the intercept was determined using

1555 MS Excel function LINEST. T: temperature; sal: salinity.

Relationship	Slope	Intercept	R^2	p-value (95% confidence)
Na-T	0.0000097 ± 0.0000037	0.00009 ± 0.00004	0.44	0.02
Na-sal	0.0000065 ± 0.0000024	-0.00009 ± 0.00008	0.44	0.015
Mg-T	0.00021 ± 0.00004	-0.0011 ± 0.0004	0.79	0.004
Mg-sal	0.00014 ± 0.00003	-0.0033 ± 0.0009	0.76	0.001

1556
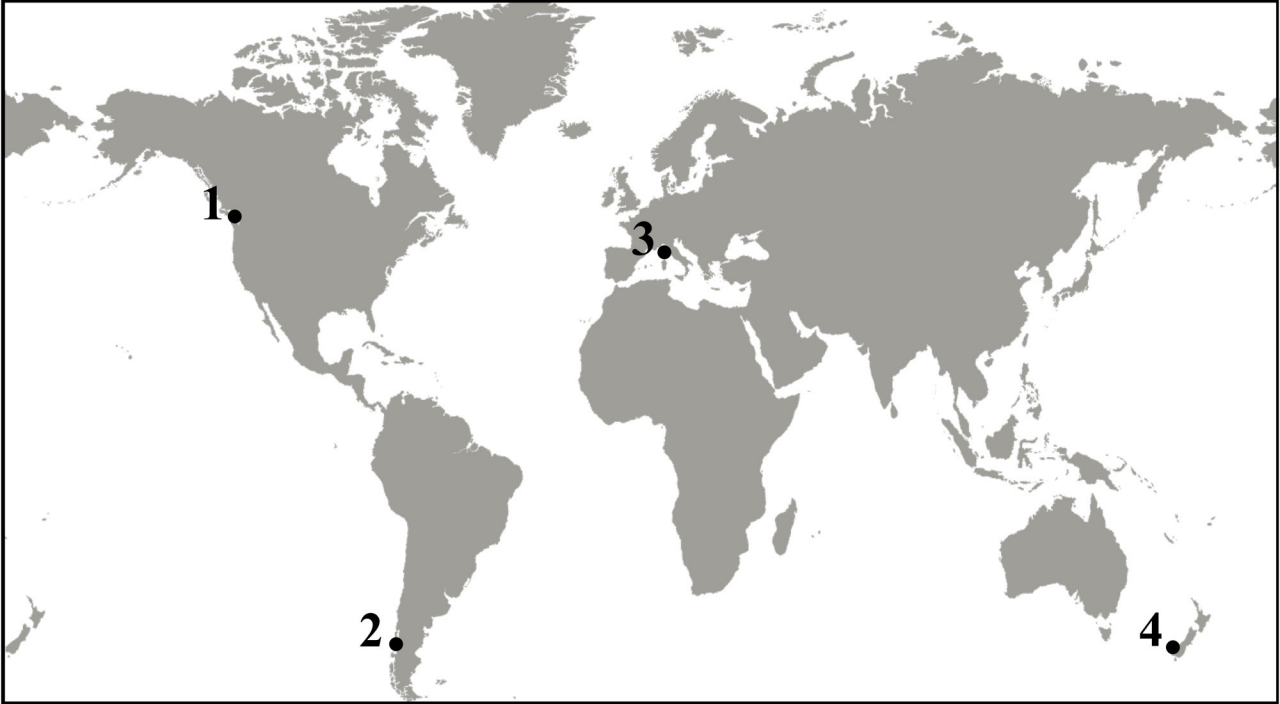
Ventral and/or dorsal valves
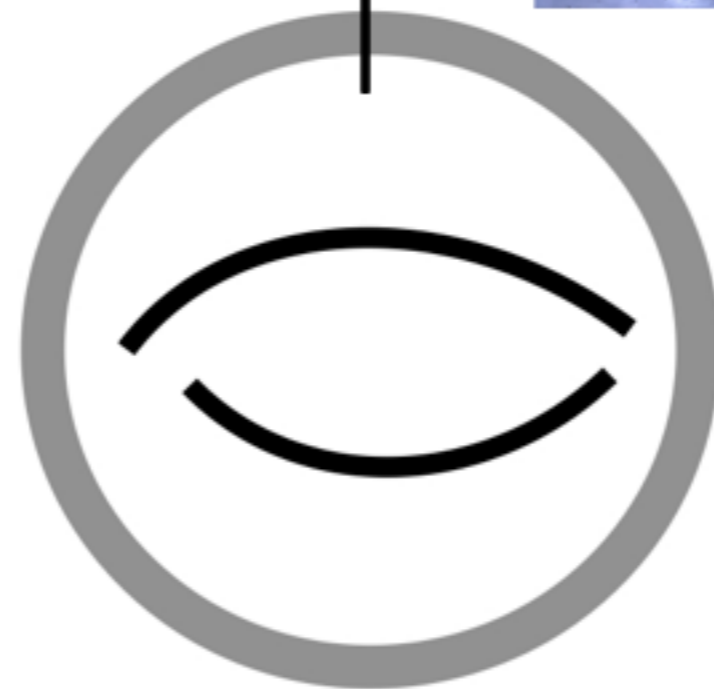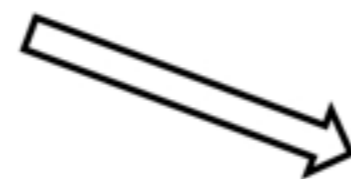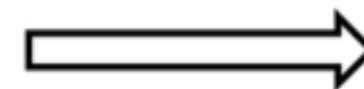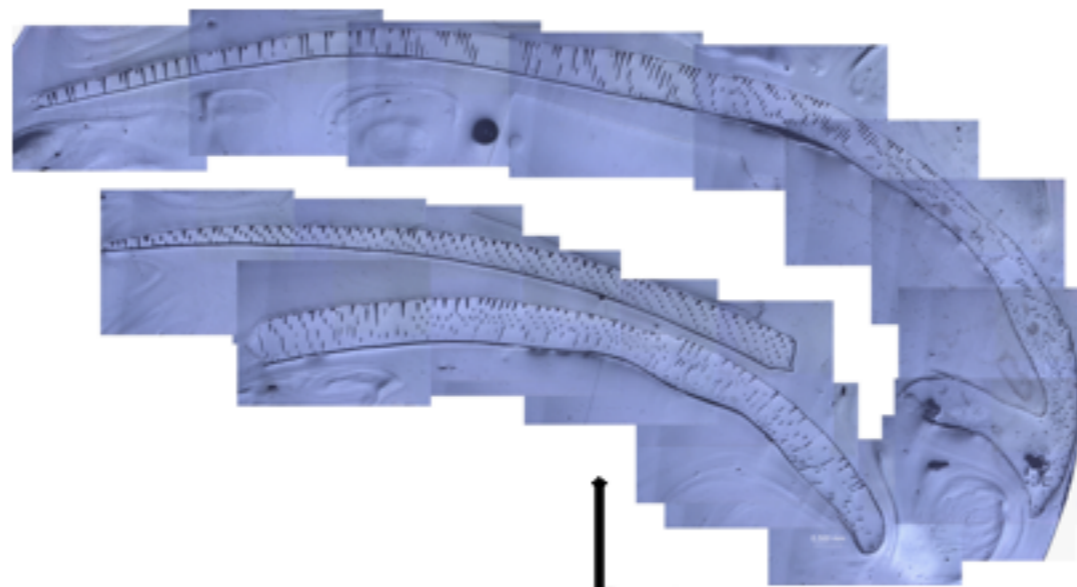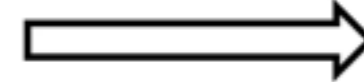
SEM
Ion Probe
± LA-ICP-MS

Powder

$\delta^{18}O$
Bulk technique

1 mm

Central

Posterior

Anterior

100μm

a) *T. transversa*
b) *M. sanguinea*
c) *M. venosa*
d) *N. nigricans*
e) *L. neozelanica*
f) *G. vitreus*

δ¹⁸O (‰ V-PDB)

Relative distance (%)

a) *M. sanguinea*
b) *N. nigricans*
c) *G. vitreus*
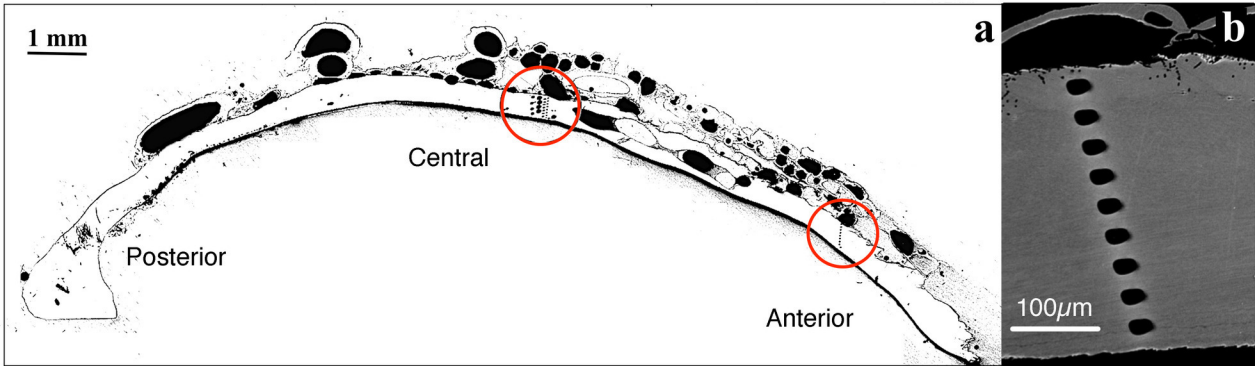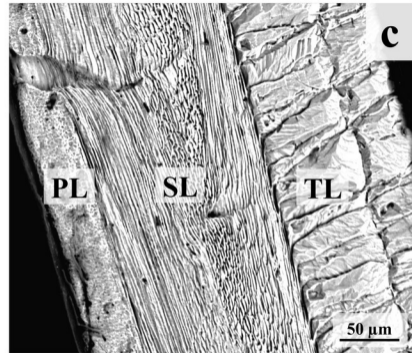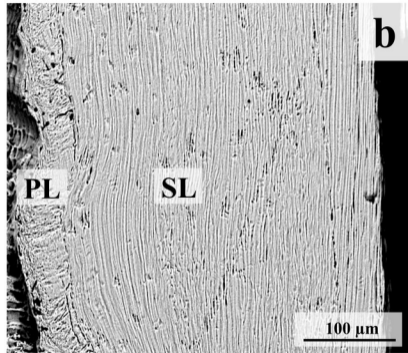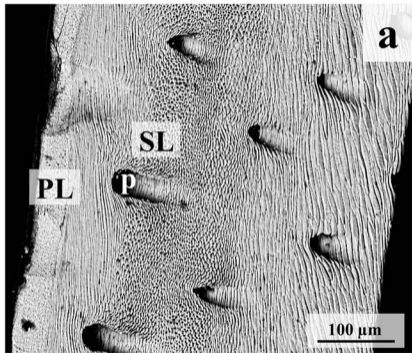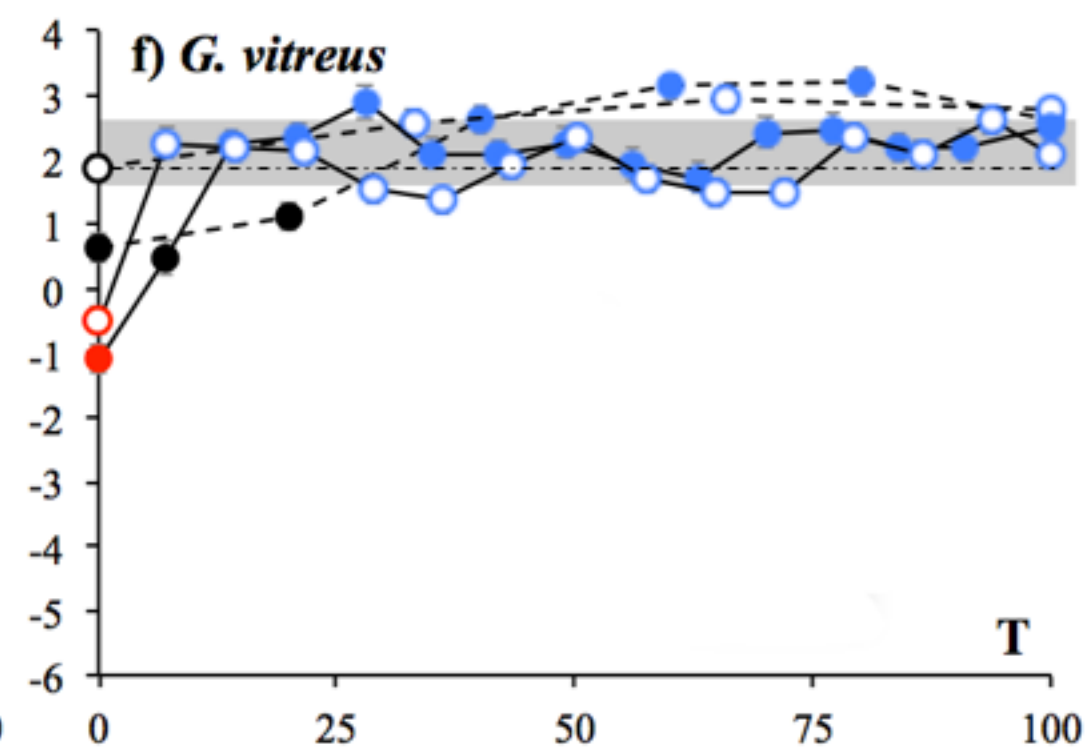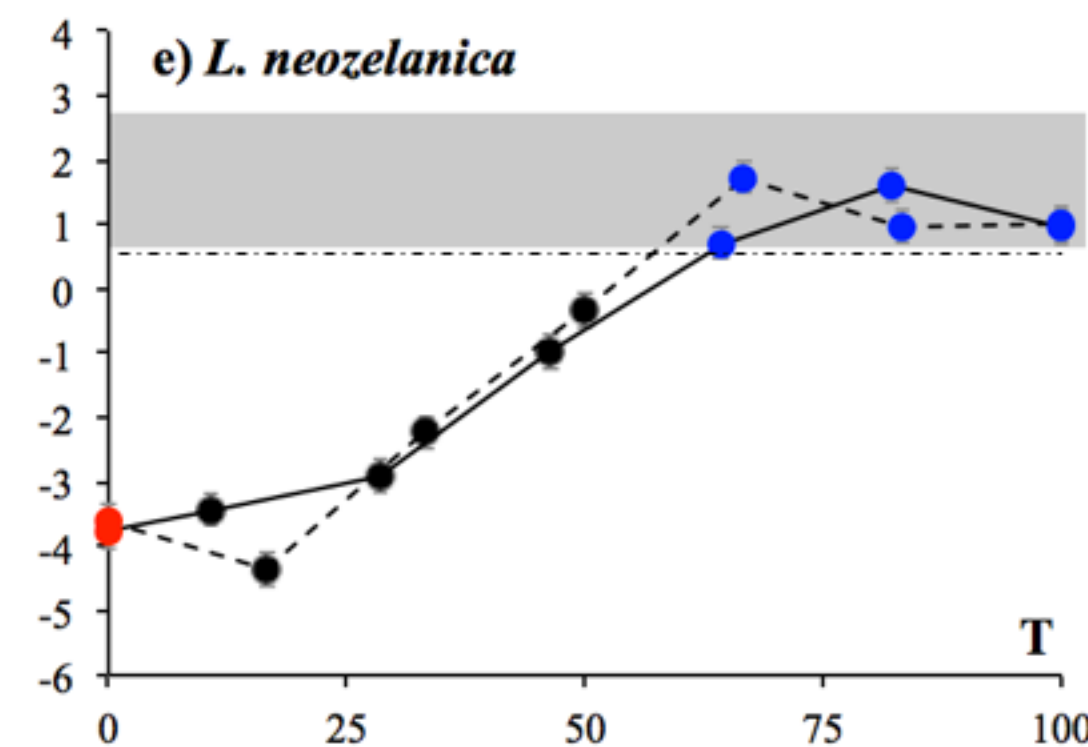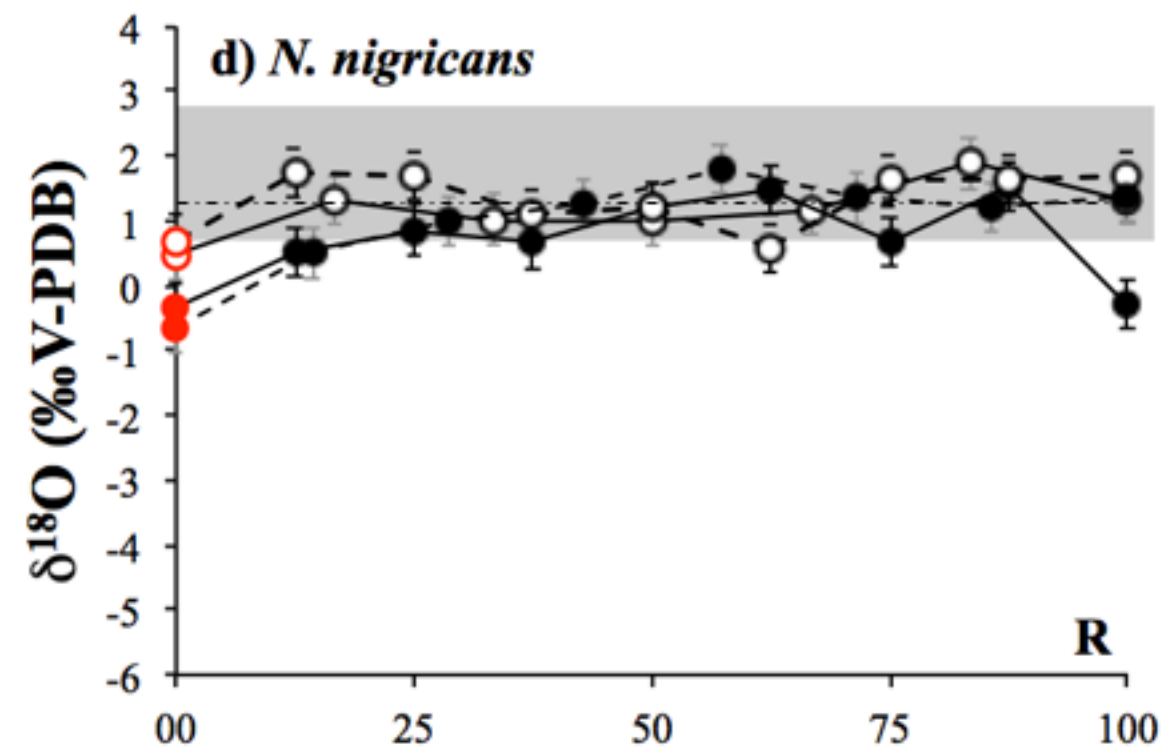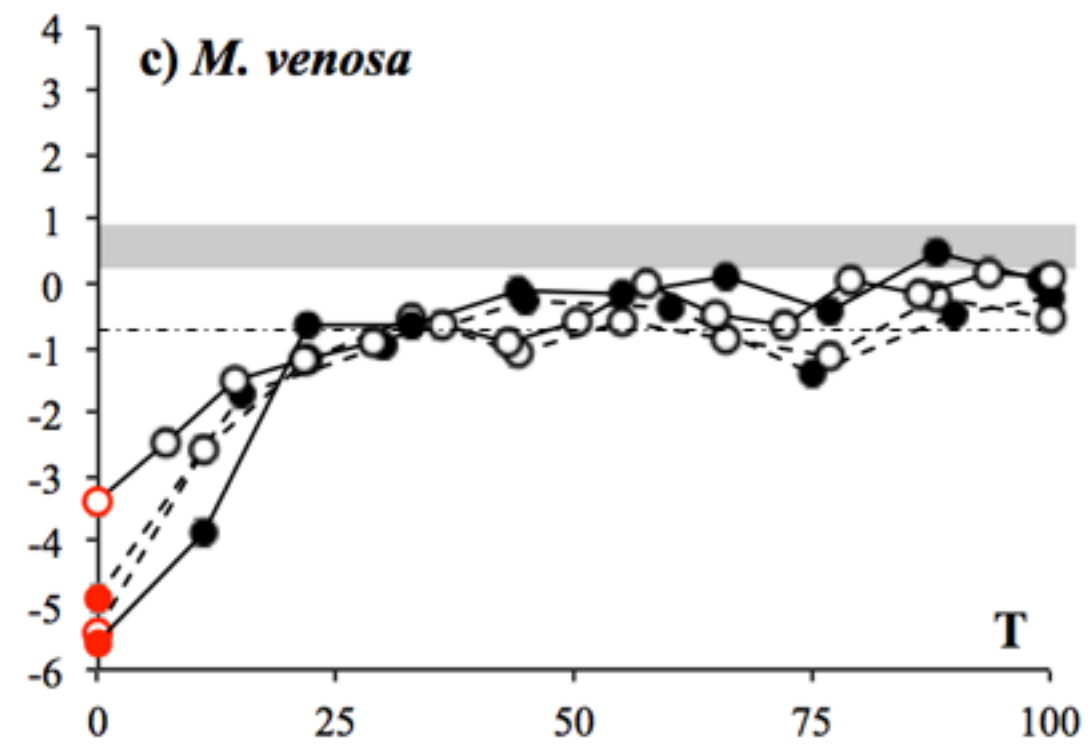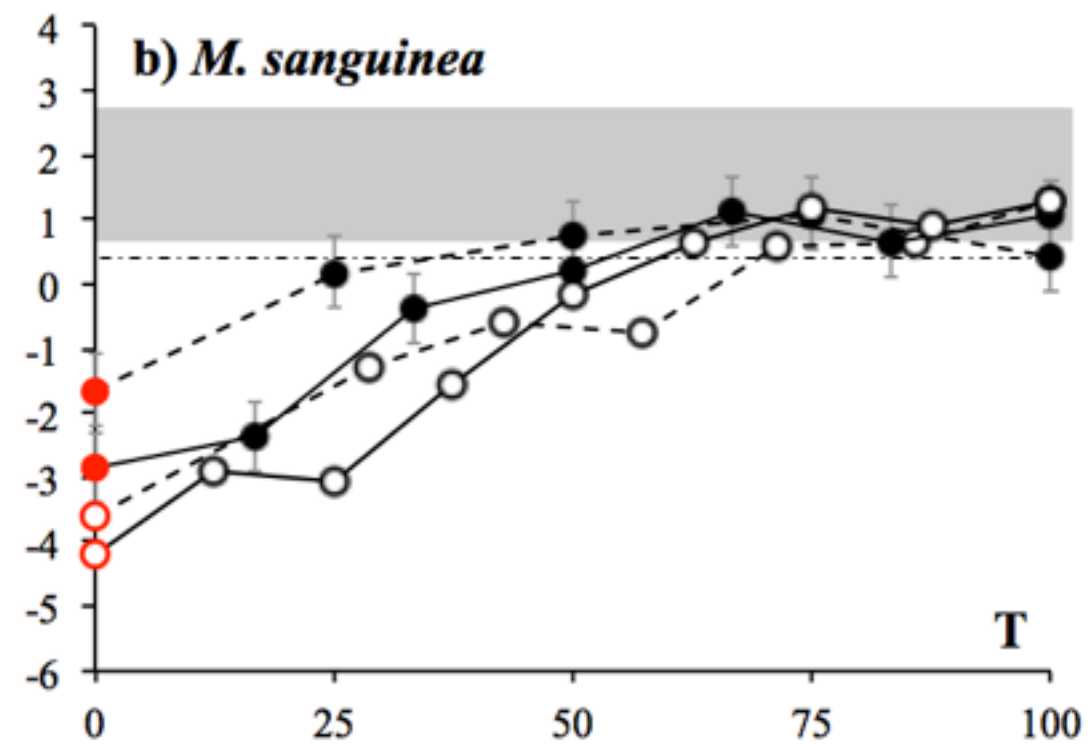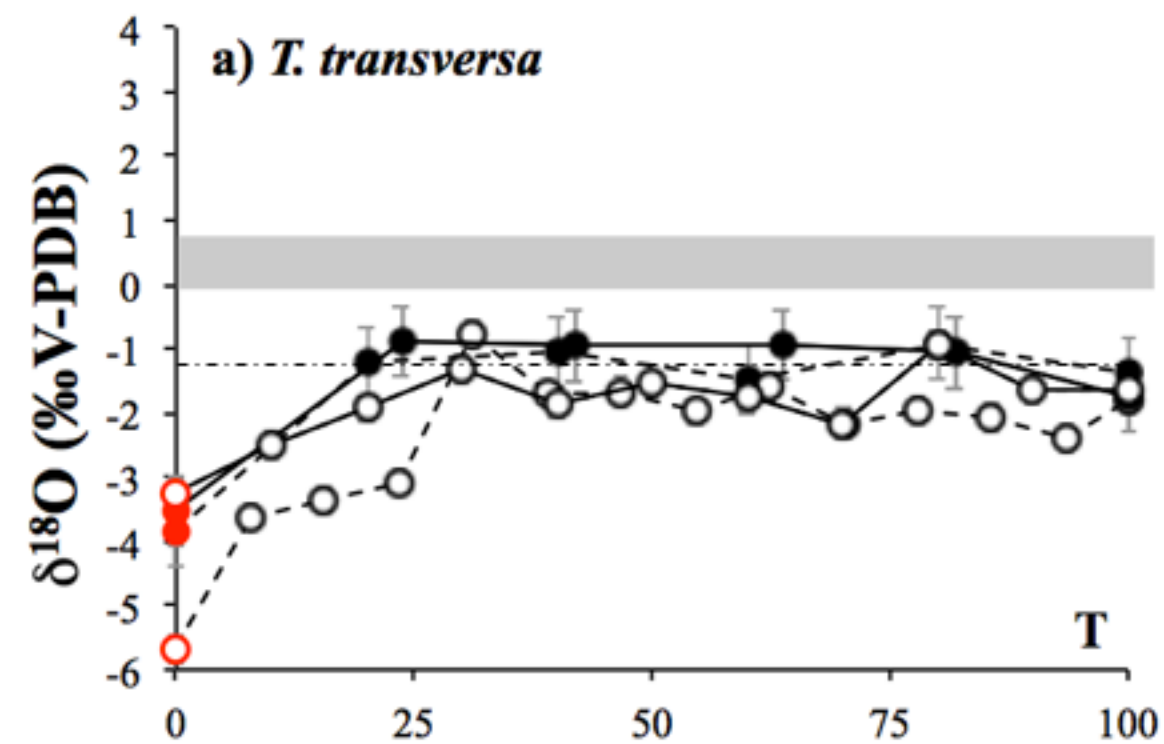
a) *T. transversa*

b) *M. sanguinea*

c) *M. venosa*

d) *N. nigricans*

e) *L. neozelanica*
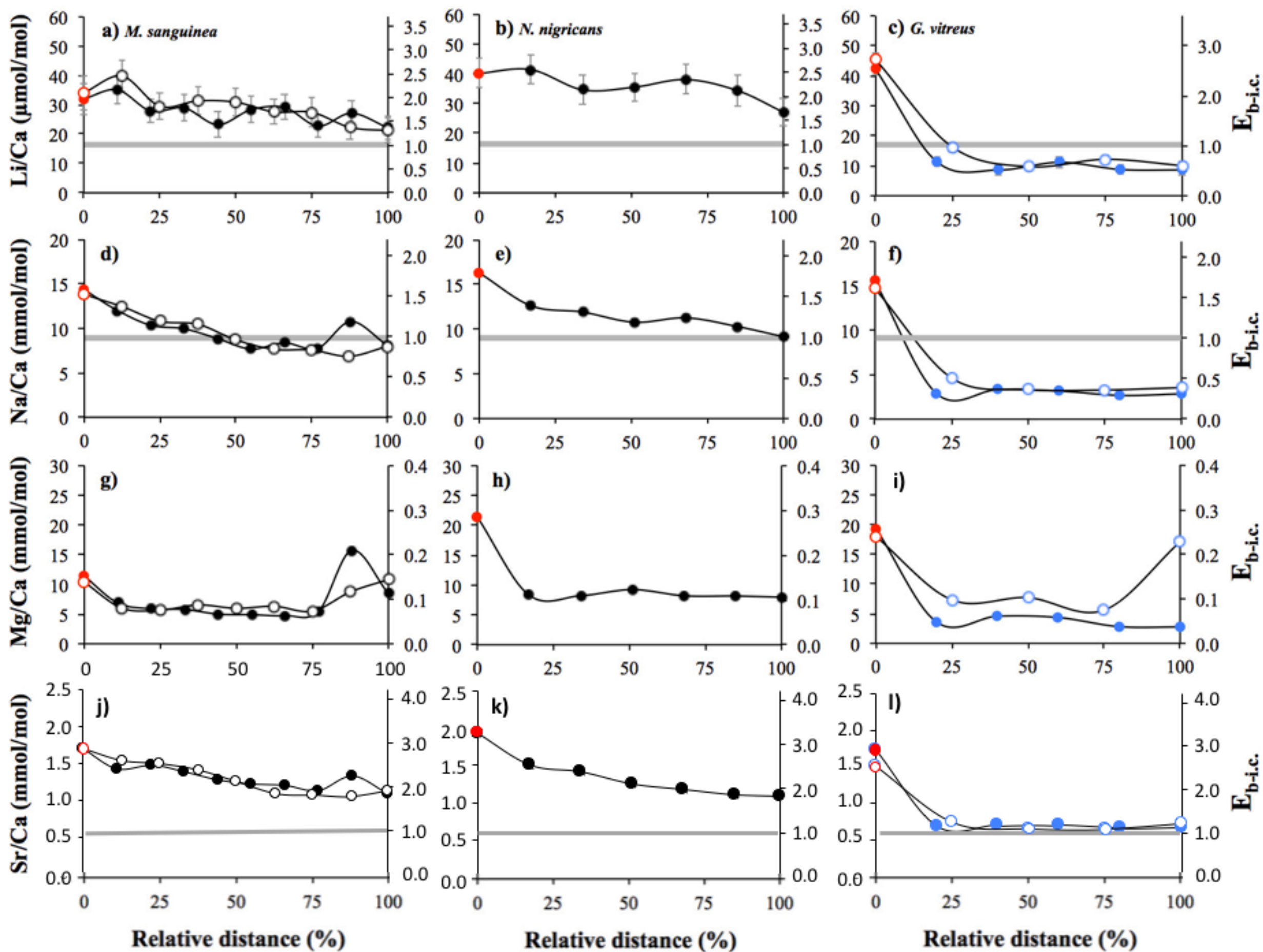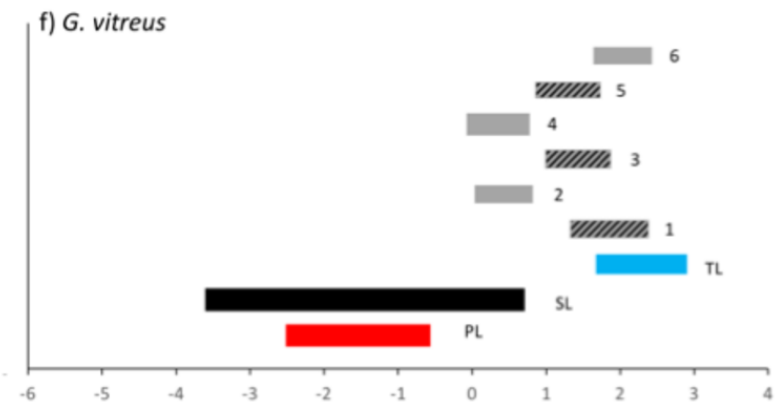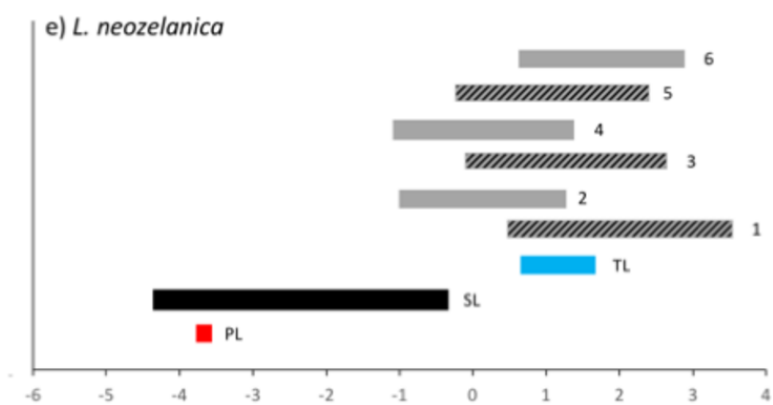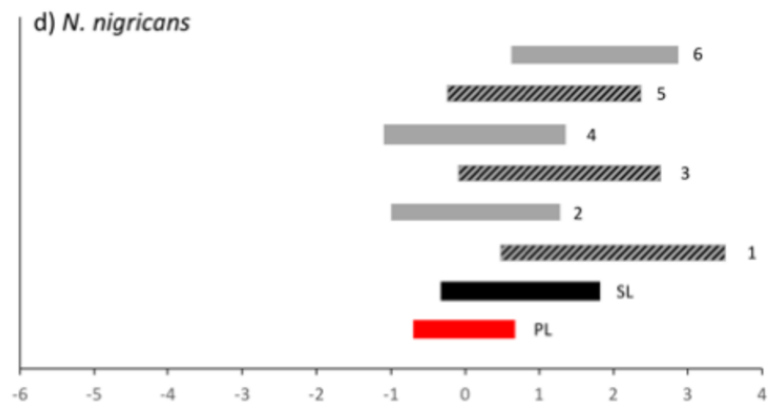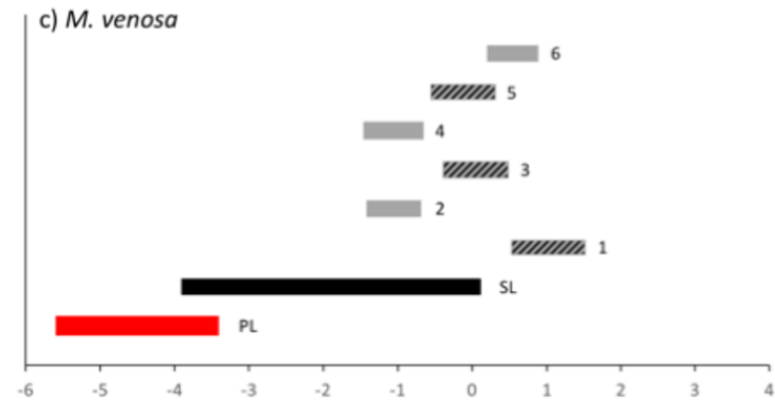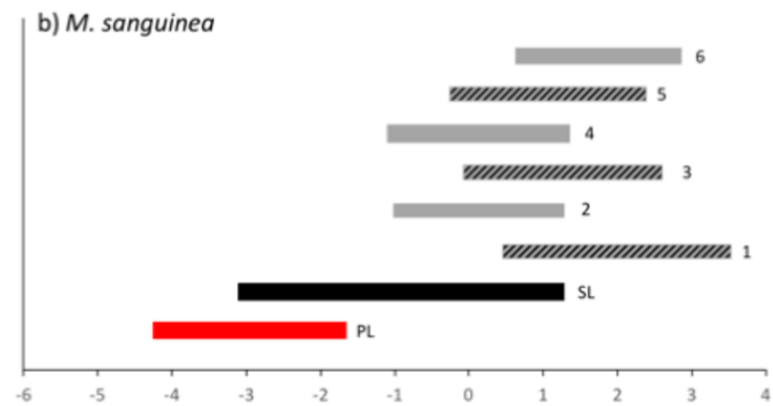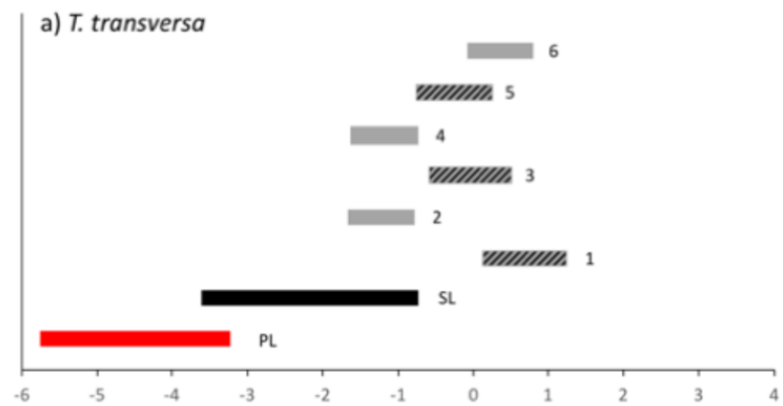
f) *G. vitreus*

$\delta^{18}O$ (‰, V-PDB)

$\delta^{18}O$ (‰, V-PDB)

$\delta^{18}O$ (‰, V-PDB)

Legend:
- ● T. transversa (blue)
- ● M. sanguinea (red)
- ● C. inconspicua (green)
- ● L. neozelanica (yellow)
- ● M. venosa (orange)
- ● G. vitreus (teal)
- ◆ N. nigricans (purple diamond)
- ✕ T. transversa (Ullmann et al., 2017)
- ✕ C. inconspicua (Ullmann et al., 2017)
- ✕ N. nigricans (Ullmann et al., 2017)

a) Sr/Ca (mmol/mol) vs δ¹⁸O (‰ V-PDB)

b) Sr/Ca (mmol/mol) vs Na/Ca (mmol/mol)
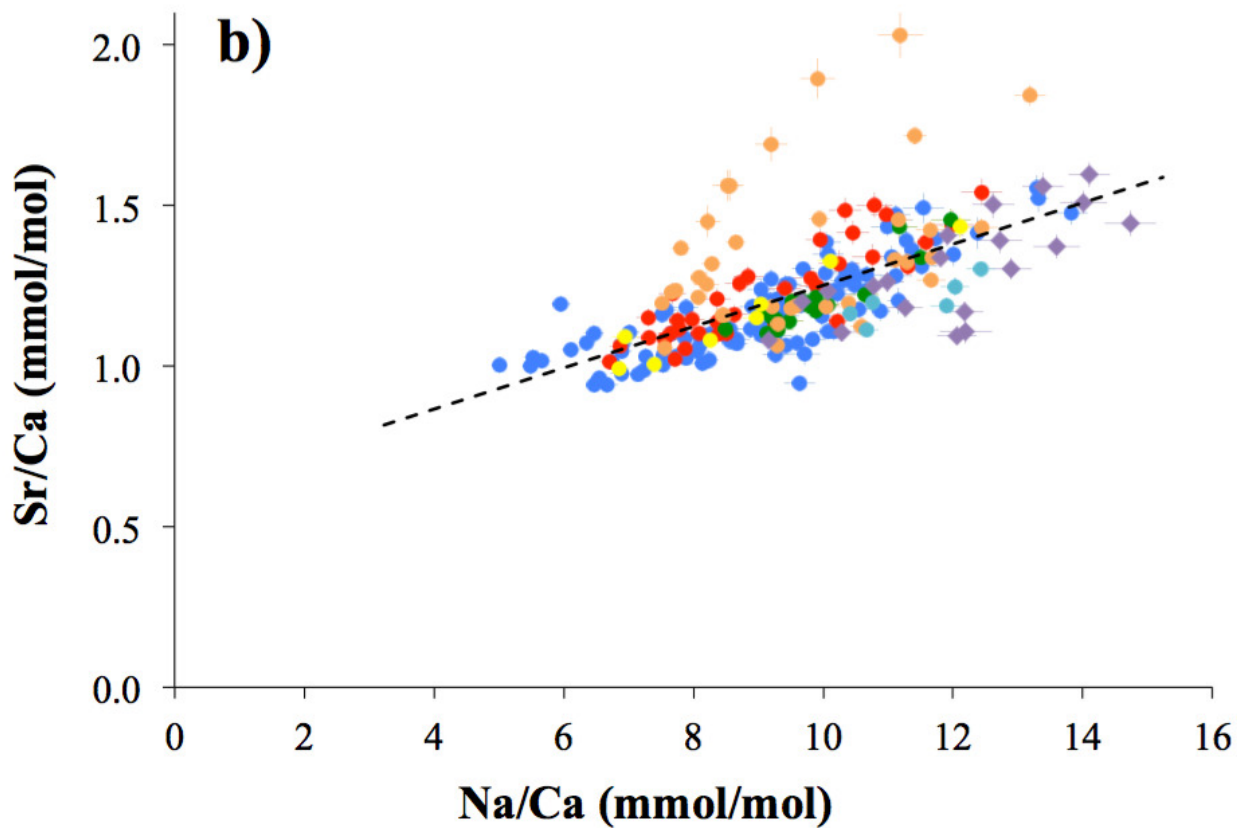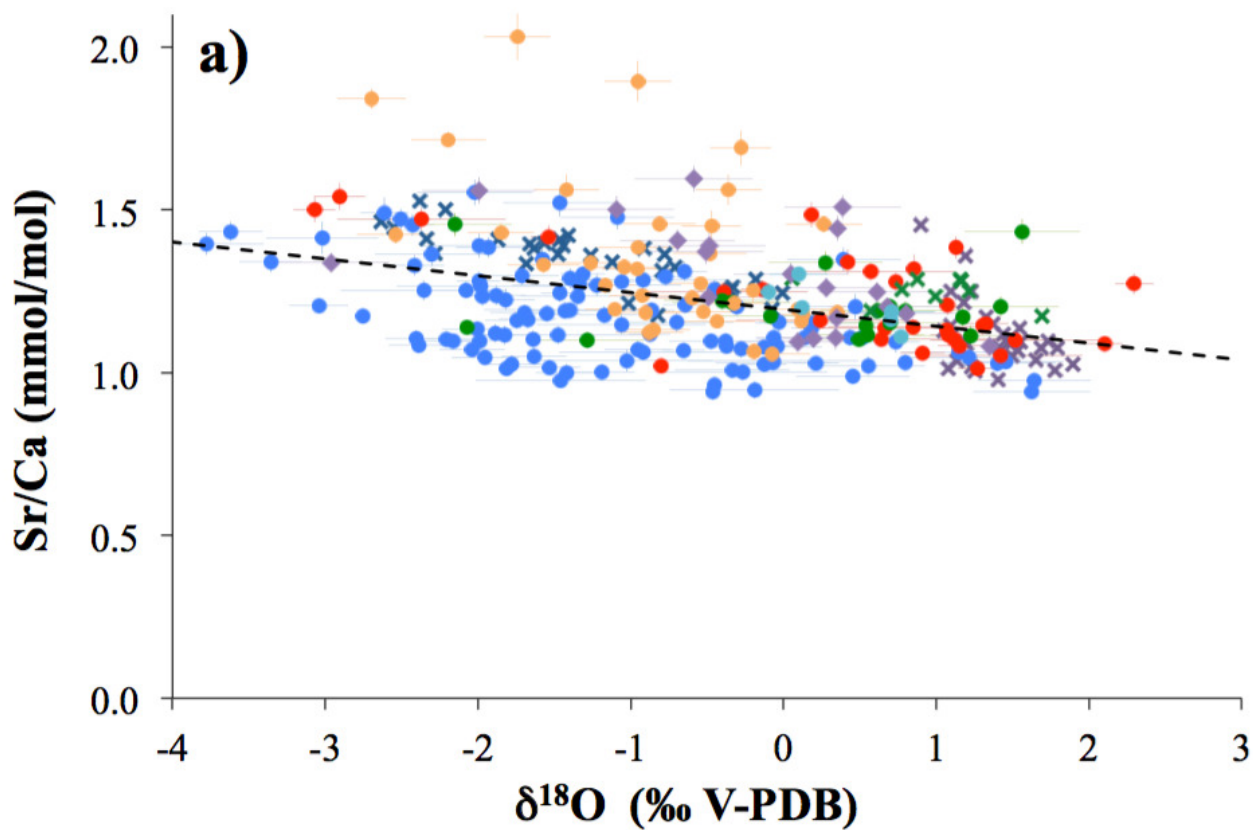
Legend (top of figure):
- T. transversa
- C. inconspicua
- M. venosa
- N. nigricans
- M. sanguinea
- L. neozelanica
- G. vitreus
- Brachiopods, other studies
- Inorganic calcite

Panel a:
$y=0.017e^{-0.03x}$
$R^2=0.67$
$y=0.012e^{-0.05x}$
$R^2=0.99$

Panel d:
Slope: $9.7\times10^{-6}\pm3.7\times10^{-6}$
Intercept: $9\times10^{-5}\pm4\times10^{-5}$
$R^2=0.44$

Panel f:
Slope: $6.5\times10^{-6}\pm2.4\times10^{-6}$
Intercept: $-9\times10^{-5}\pm8\times10^{-5}$
$R^2=0.44$

Panel g:
GB-Mg

Y-axis labels: D_{Li}, D_{Na}, D_{Mg}, D_{Sr}

X-axis labels: Temperature (°C), pH, Salinity